Continuum-molecular modeling of planar micropolar media: Anisotropy, chiral properties and length-scale effects

Vito Diana *, Andrea Bacigalupo, Luigi Gambarotta

Department of Civil, Chemical and Environmental Engineering, University of Genova, Genoa, Italy

ARTICLE INFO

ABSTRACT

This paper presents a continuum-molecular formulation for bi-dimensional micropolar media within the mathematical formalism of a revised peridynamic theory with oriented material points. A variational procedure is considered to derive the fundamental governing equations of the model, which postulates that material points interact through pair potentials allowing generalized pairwise actions to be derived as energy conjugates to properly defined pairwise deformation measures. While continuity of mass is assumed, constitutive laws are produced for long-range micro-interactions to reproduce the effective behavior of the material at the macro-scale. The definition of proper micromoduli functions respecting material symmetries and invariance properties allows then to obtain a non-local micropolar continuum based on pseudo-discrete kinematics, while providing a mechanism-based description of material anisotropy and coupling behaviors uncovered by classical elasticity. An analytic micro-macro moduli correspondence procedure is also established, based on the formal analogy with the constitutive tensor of centrosymmetric planar micropolar continua. As an important result of this research, we show that distinctive chiral effects of micropolar elasticity can be reproduced by introducing a directional independent pseudo-scalar pair potential, which turns out to be analytically vanishing when the rotationally invariant part of the corresponding continuum elastic tensor is invariant to mirror reflections as well. Moreover, the proposed formulation demonstrates sensitivity to elastic bending size-effect as specific property of structured materials homogenized as micropolar continua, and related to the characteristic length of their underlying microstructure. The resulting *constitutive* non-locality, which plays an important role in fracture problems, is conceptually separated with respect to the *intrinsic* non-local character of the model related to the integral nature of its governing equations, and then does not vanish when the horizon reduces to zero. The theoretical findings and the effectiveness of the model are successfully verified through illustrative examples referred to representative cases of structured materials homogenized as micropolar continua, including length-scale dependent quasi-static crack propagation as well as the mechanism-based description of the coupling between bulk strain and micro-rotation in elastic bi-dimensional homogenized chiral lattices.

1. Introduction

Molecular models and related structure theories have been proposed in solid mechanics with the aim of providing a mechanism-based description of the elastic and inelastic behavior of materials at the observation scale, by using the concept of generalized distance force as ultimate action (Love, 1944; Diana, 2023). The first models of this kind, developed by French mathematicians of the nineteenth century, were based on the hypothesis of central forces depending only on the mutual distance between pairs of *molecules*. The latter were regarded as simple centers of forces endowed with the property of mass, their displacement being defined by a vector field in the continuum of Euclidean geometry associated with the corresponding elastic body (Love, 1944; Capecchi

and Ruta, 2015). As a consequence of the assumed structure theory, an internal constrain holds for constitutive equations, namely the Cauchy relation(s), which causes the number of independent elastic constant in standard bi-dimensional solids to reduce to five. This drawback was later overcome by Voigt (1900), whose structure theory postulated oriented molecules interacting in pairs via a system of actions derivable from a scalar quadratic pair potential, and reducible to a force and a couple (Capecchi et al., 2010). The resulting governing equations of the molecular model, which assigns an auxiliary role to the physical concept of continuum, do not necessarily verify the Cauchy relation, the corresponding elastic constants being six in the most general two-dimensional case. Nevertheless, the mechanism-based view was

---

* Corresponding author.
  E-mail address: vito.diana@unige.it (V. Diana).

abandoned in favor of the phenomenological approach of (classical) Continuum Mechanics or local field theory (Truesdell, 1992), which has provided over time the foundation for well-established models of the mechanical response of solids at the meso- and macro-scale (Truesdell and Toupin, 1960). However, several important phenomena observed in mechanical tests such as elastic size-effect and dispersion of elastic waves in materials due to their microstructure heterogeneity turn out to be unpredictable by local field theory (Mindlin et al., 1963; Kunin, 1982). These considerations led several mathematicians of twentieth century towards the introduction of additional kinematic degrees of freedom of rigid bodies, to describe the arrangement of material microstructure (Di Paola et al., 2013; Cosserat and Cosserat, 1909; Eringen, 1966a), and towards the development of refined non-local field theories, constructed on a phenomenological basis, involving gradients or integrals of the strain field in the constitutive equations to account for the inhomogeneity of the material at a lower scale (Mindlin and Eshel, 1968; Eringen and Edelen, 1972; Green and Rivlin, 1964). Specifically, the enriched kinematics proper of oriented media or polar field theories (Cosserat and Cosserat, 1909; Eringen, 1966a, 1972), which traces back to Voigt studies on crystals (Voigt, 1887), naturally lends itself to the elastic multiscale modeling of discrete and lattice-like materials such as modern periodic architectured solids made up of lumped masses/rigid blocks and elastic ligaments/interfaces, as the additional micro-rotation field turns out to be kinematically consistent with the discrete Lagrangian description of the corresponding microstructures (Bacigalupo and Gambarotta, 2017). Moreover, besides length-scale sensitivity, micropolar elasticity (through continualization schemes) has been also proved useful to provide a synthetic and effective description of several unusual behaviors uncovered by classical Continuum as well as exotic properties of great engineering interest in bi-dimensional mechanical metamaterials, such as auxetics, high compressibility, etc. Liu et al. (2012), Chen et al. (2014b), Bacigalupo and Gambarotta (2020), Diana et al. (2023), Cui and Ju (2022), Fleck et al. (2010), Prall and Lakes (1997). Recently, research interest in this field has extended to the design and modeling of periodic lattices with kinking prohibition directions (Huang et al., 2023), high fracture toughness micro-architectured materials (Liu et al., 2020; Fleck and Qiu, 2007; Quintana-Alonso and Fleck, 2009; Omidi and St-Pierre, 2023), and indentation resistant microstructures (Evans and Alderson, 2000). However, it is well known that field theories are, in general, limited in their ability to describe problems involving (possibly evolving) geometric discontinuities and spontaneous formation of cracks in solids, as a direct consequence of the intrinsic requirements of their governing equations involving spatial derivatives. Important and relatively recent contributions in the attempt of bridging the views of field and structure theories were given, among others, by Kröner (1967) and Kunin (1982). Later, Tadmor et al. (1996) presented a quasicontinuum approach for defect analysis in solids, whereas Gao and Klein proposed an integration of continuum models with cohesive surfaces and molecular models with virtual bonds for fracture problems (Gao and Klein, 1998). In this context, a general theory of solid mechanics, namely Peridynamics, based on actions at a distance and formulated in terms of integro-differential equations without partial derivatives in space, was proposed by Silling (2000). The range of forces and the continuity of matter being two different concepts (Kröner, 1967), the original (bond-based) model postulated material points in a continuum interacting through pairwise vector valued central force functions. Hence, although it represented a generalization of the early structure theory (Love, 1944) to include discontinuities and non-locality in an explicit form, Cauchy relations were not evaded (Silling, 2000). The strategy proposed later to overcome this restriction and to enlarge the scope of applicability of the model consisted in the introduction of proper point-wise defined deformation measures, force functions and multi-body potentials (state-based type (Silling et al., 2007; Warren et al., 2009) and continuum-kinematic inspired formulations (Javili et al., 2019)). As a different approach, Gerstle et al. (2007) maintained

the pairwise formalism of bond-based type equations while endowing material points with additional kinematic descriptors, the assumed kinematic of pair interactions steming from that of a virtual Euler–Bernoulli beam. In the spirit of Voigt structure theory, Diana and Casolo (2019) proposed instead an oriented peridynamic continuum-molecular model based on a generalized kinematic employing the definition of a non-central pair potential consisting of three independent terms, quadratic functions of equal number of pairwise deformation measures (Diana, 2023). This approach has been followed by later works, and applied to the reduced case of isotropic and anisotropic standard elasticity (Diana, 2023; Diana et al., 2022). The enriched kinematics and the specific features characterizing the above referenced oriented continuum-molecular formulation (Diana, 2023) allows for its natural extension to micropolar elasticity and then to a consistent description of length-scale sensitivity, overall *shear anisotropy* and other micropolar effects in micro-architectured solids such as periodic lattice-like materials (Diana et al., 2023; Bacigalupo and Gambarotta, 2017; Casolo, 2021). Previous studies of this kind on micropolar media, most based on mechanical formulations featuring multi-body potentials, only consider the particular case of isotropic materials (Chen et al., 2019; Chowdhury et al., 2015; Zhou et al., 2023; Wan et al., 2022), whereas a general constitutive modeling strategy for chirality (i.e. lack of invariance with respect to mirror reflection resulting in the absence of axes of reflection symmetry) in bi-dimensional micropolar solids is not available. It can be noted that the pairwise formalism may provide an intuitive mechanism-based description of overall macro properties of materials, at the same time being closely related to the mechanics of full-discrete models for lattice-like mechanical metamaterials (Diana et al., 2023; Diana, 2023). In a computational context, pair-potential based continuum-molecular (peridynamic) models lead to mathematical formulations resulting in an easier implementation and higher computational efficiency compared to models based on multi-body potentials as state-based type models (Boys et al., 2021). Actually, their use is preferred, when possible, as the large number of literature works on bond-based models demonstrates. It is reminded here that micropolar elasticity is specifically sensitive to chirality (Chen et al., 2014b; Prall and Lakes, 1997; Auffray et al., 2022). In particular, differently from standard elasticity, hemitropy (invariance under arbitrary proper orthogonal transformations, e.g. SO(2) invariance) of the constitutive tensor does not necessarily implies its isotropy (invariance under arbitrary orthogonal transformations, e.g. O(2) invariance) in micropolar continua (Auffray et al., 2022). Actually, as it can be shown by invoking the hierarchical structure of bi-dimensional micropolar elasticity tensors (Zou et al., 2001), this intrinsic feature enables the appearance of hemitropic solids (also referred to as *isotropic chiral* (Liu et al., 2012)) as well as *orthotropic chiral* solids (Chen et al., 2014b; Bacigalupo and Gambarotta, 2020, 2014; Giorgio et al., 2022). Considering that the coupling between the *bulk* deformation and independent nodal rotation is the reason for many unusual behaviors observed in periodic chiral lattice-like materials and metamaterials, such as auxetics, high compressibility, etc., micropolar theory can provide an intuitive and effective description of their overall behavior (Chen et al., 2014b; Diana et al., 2023). Furthermore, while for tri-dimensional solids non-centrosymmetric micropolar continuum theory is usually used to capture chiral effects, in the bi-dimensional case non-centrosimmetry (i.e. lack of invariance with respect to inversion) and chirality turn out to be analytically decoupled (Liu et al., 2012; Bacigalupo and Gambarotta, 2017; Auffray et al., 2022). It is worth considering that inversion in two-dimensions is a rotation by π, while in three dimensions it is defined by an improper transformation (Auffray et al., 2022).

This paper proposes a generalized continuum-molecular formulation for bi-dimensional centrosymmetric chiral and achiral structured materials homogenized as micropolar media. The micropotential functions allow modeling chirality as well as bending size-effect and elastic
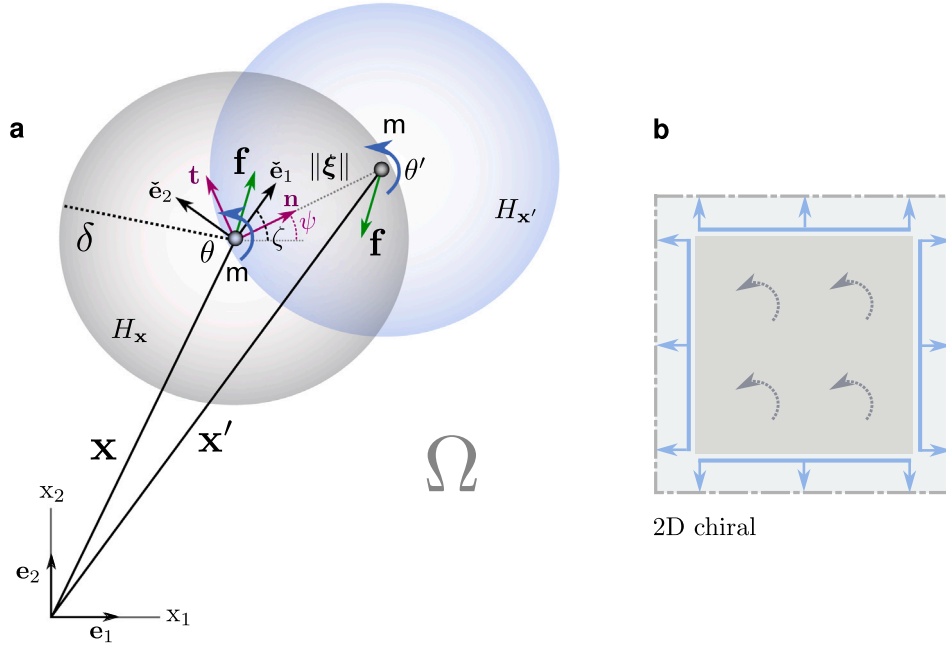
Fig. 1. Detail of the interaction between the oriented material point **x** and the generic oriented material point $\mathbf{x}' \in H_\mathbf{x}$ (**a**); Typical elastic coupling between axial/bulk strain and micro-rotation in bi-dimensional hemitropic micropolar solids (**b**).

anisotropy in homogenized micropolar solids while using pairwise descriptions of deformation and constitutive properties. We demonstrate that a mechanism-based description of specific chiral properties owing to SO(2) invariance can be obtained in a rigorous form by introducing a properly-defined direction-independent pseudo-scalar pair-potential. Moreover, because of the adopted pairwise formalism, we show essential analogies between continuum-molecular mathematical models and real lattice-like materials that can provide new insight for the design of modern micro-architectured solids endowing exotic mechanical properties. Finally, the influence of the characteristic length in bending – a property related to the size of the underlying microstructure – during crack nucleation and propagation in micropolar media is investigated. The paper is organized as follows: Kinematics and field equations of the oriented continuum-molecular model are defined in Section 2. The constitutive model and the general micro-macro correspondence procedure for anisotropic chiral and achiral micropolar elasticity is detailed in Section 2.1 and Section 2.1.1, respectively. Benchmark problems and validation examples involving materials of different symmetry classes are presented in Section 3.

2. The oriented continuum-molecular model

Let us consider a two-dimensional continuum solid body Ω, composed of oriented material points **x**. Material points **x** and **x**' within a finite distance (namely the *horizon* δ (Silling, 2000)), are assumed to interact with each other through non-central pairwise actions depending on pairwise constitutive parameters and pairwise deformation variables (Fig. 1). The set of all material points $\mathbf{x}' \in \Omega$ such that $\|\mathbf{x}' - \mathbf{x}\| \leq \delta$ is denoted by $H_\mathbf{x}$, which defines the horizon region of material point **x**. The generic vector $\boldsymbol{\xi} = \mathbf{x}' - \mathbf{x}$ is called *bond* (Silling, 2000) or virtual fiber. A theoretical (peridynamic) model of this kind is here referred to as *oriented* continuum-molecular (CM) model (Diana, 2023). Given the reference orthonormal basis $\{\mathbf{e}_1, \mathbf{e}_2\}$, the body configuration at time t is described by the displacement field $\mathbf{u}(\mathbf{x}, t) = u_i \mathbf{e}_i$ and rotation field $\theta(\mathbf{x}, t)$ defined over Ω. The applied body forces and couples are denoted by $\boldsymbol{b}(\mathbf{x}, t)$ and $c(\mathbf{x}, t)$, respectively, and are assumed conservative. The scalar-valued constant functions $\rho(\mathbf{x}, t) = \rho$ and $\varrho(\mathbf{x}, t) = \varrho$ denote instead the densities of mass and mass moment of inertia, respectively. We define three linearized pairwise deformation measures, depending on

the relative position $\boldsymbol{\xi} = \mathbf{x}' - \mathbf{x}$, relative displacement $\boldsymbol{\eta} = \mathbf{u}(\mathbf{x}', t) - \mathbf{u}(\mathbf{x}, t) = \mathbf{u}' - \mathbf{u}$ and rotations $\theta(\mathbf{x}, t) = \theta$ and $\theta(\mathbf{x}', t) = \theta'$ of the generic pair of interacting material points (Diana and Casolo, 2019). Specifically, the deformation in the direction $\mathbf{n} = \boldsymbol{\xi}/\|\boldsymbol{\xi}\|$ defined by the generic virtual fiber is the pairwise stretch s,

$$s(\mathbf{x}, \mathbf{x}', t) = \frac{\boldsymbol{\eta} \cdot \mathbf{n}}{\|\boldsymbol{\xi}\|} = \frac{\eta_\mathrm{n}}{\|\boldsymbol{\xi}\|} \tag{1}$$

with $\eta_\mathrm{n} = u'_\mathrm{n} - u_\mathrm{n}$ being the component of the vector $\boldsymbol{\eta}$ along the unit vector **n**. The pairwise shear or angular deformation is defined as

$$\gamma(\mathbf{x}, \mathbf{x}', t) = \frac{\boldsymbol{\eta} \cdot \mathbf{t}}{\|\boldsymbol{\xi}\|} - \frac{\theta' + \theta}{2} = \frac{\eta_\mathrm{t}}{\|\boldsymbol{\xi}\|} - \bar{\theta} \tag{2}$$

where, since $\eta_\mathrm{t} = u'_\mathrm{t} - u_\mathrm{t}$ is the component of $\boldsymbol{\eta}$ along the unit vector $\mathbf{t} : \mathbf{t} \perp \mathbf{n}$ (Fig. 1), the shear deformation can be interpreted as the difference between the linearized rotation angle of the virtual fiber $\eta_\mathrm{t}/\|\boldsymbol{\xi}\|$ and the average rotation $\bar{\theta}$ of the corresponding pair of oriented material points **x** and **x**'. The third pairwise deformation variable turns out to be function instead of the relative rotation of two interacting oriented material points according to the dimensional ratio

$$\chi(\mathbf{x}, \mathbf{x}', t) = \frac{\theta' - \theta}{\|\boldsymbol{\xi}\|} = \frac{\vartheta}{\|\boldsymbol{\xi}\|} \tag{3}$$

which can be rather interpreted as the average curvature of the generic virtual fiber.

The elastic pair potential or micropotential function for energy conserving materials can be defined as

$$\mathrm{w}(\mathbf{x}, \mathbf{x}', t) = \left[\mathrm{w}_s(\mathbf{x}, \mathbf{x}', t) + \mathrm{w}_\gamma(\mathbf{x}, \mathbf{x}', t) + \mathrm{w}_{s\gamma}(\mathbf{x}, \mathbf{x}', t) + \mathrm{w}_\chi(\mathbf{x}, \mathbf{x}', t)\right]$$
$$= \frac{1}{2} \Lambda(\mathbf{x}, \mathbf{x}')\|\boldsymbol{\xi}\| \left[k_\mathrm{n} s^2 + k_\mathrm{t} \gamma^2 + 2k_\mathrm{a} s\gamma + k_\mathrm{b} \chi^2\right] \tag{4}$$

such that the scalar-valued mutual actions between pairs of oriented material points result to be work-conjugate to the pairwise deformation measures defined above, and then obtained as

$$f_\mathrm{n}(\mathbf{x}, \mathbf{x}', t) = \frac{\partial w(\mathbf{x}, \mathbf{x}', t)}{\partial s} = \frac{\partial \mathrm{w}(\mathbf{x}, \mathbf{x}', t)}{\partial \eta_\mathrm{n}} = \Lambda(\mathbf{x}, \mathbf{x}')[k_\mathrm{n} s + k_\mathrm{a} \gamma] \tag{5}$$

$$f_\mathrm{t}(\mathbf{x}, \mathbf{x}', t) = \frac{\partial w(\mathbf{x}, \mathbf{x}', t)}{\partial \gamma} = \frac{\partial \mathrm{w}(\mathbf{x}, \mathbf{x}', t)}{\partial \eta_\mathrm{t}} = \Lambda(\mathbf{x}, \mathbf{x}')[k_\mathrm{t} \gamma + k_\mathrm{a} s] \tag{6}$$

$$m_\mathrm{b}(\mathbf{x}, \mathbf{x}', t) = \frac{\partial w(\mathbf{x}, \mathbf{x}', t)}{\partial \chi} = \frac{\partial \mathrm{w}(\mathbf{x}, \mathbf{x}', t)}{\partial \vartheta} = \Lambda(\mathbf{x}, \mathbf{x}')k_\mathrm{b} \chi \tag{7}$$

where $w(\mathbf{x}, \mathbf{x}', t) = \mathrm{w}(\mathbf{x}, \mathbf{x}', t)/\|\boldsymbol{\xi}\|$ is the pairwise elastic potential energy function per unit distance $\|\boldsymbol{\xi}\|$, while $k_\mathrm{n} = k_\mathrm{n}(\mathbf{x}, \mathbf{x}') = k_\mathrm{n}(\psi)$, $k_\mathrm{t} = k_\mathrm{t}(\mathbf{x}, \mathbf{x}') = k_\mathrm{t}(\psi)$, $k_\mathrm{a} = k_\mathrm{a}(\mathbf{x}, \mathbf{x}') = k_\mathrm{a}(\psi)$ and $k_\mathrm{b} = k_\mathrm{b}(\mathbf{x}, \mathbf{x}') = k_\mathrm{b}(\psi)$ are the micromoduli functions or pairwise constitutive functions depending, in general, on the spatial orientation $\psi = \mathrm{Arg}\left(\boldsymbol{\xi} \cdot \mathbf{e}_1 + \iota \boldsymbol{\xi} \cdot \mathbf{e}_2\right)$ of the virtual fiber. In the above, $\Lambda \equiv \Lambda(\mathbf{x}, \mathbf{x}') = \Lambda(\|\boldsymbol{\xi}\|)$ is instead the influence or attenuation function, that weights the nonlocal interactions within the spatial domain $H_\mathbf{x}$ with respect to $\|\boldsymbol{\xi}\|$ (Eringen, 1966b; Seleson and Parks, 2011). Differently from the continuum-molecular formulation for standard elasticity detailed in Diana (2023), here non vanishing micro-bending potential $\mathrm{w}_\chi(\mathbf{x}, \mathbf{x}', t)$ is considered, whereas $\mathrm{w}_{s\gamma}(\mathbf{x}, \mathbf{x}', t)$ is suitably introduced for reproducing specific elastic couplings that may appear in bi-dimensional microstructured materials homogenized as chiral micropolar continua (Fig. 1) (Lakes, 2001; Liu et al., 2012; Bacigalupo and Gambarotta, 2020; Auffray et al., 2022). Because of the assumed hypothesis of centrosymmetry, there are no micropotential terms coupling the pairwise deformations defined in Eqs. (1)–(2) with that introduced in Eq. (3). As it will be discussed later, in bi-dimensional solids chirality is due to the absence of lines of material reflection symmetry, a property that reflects itself in a particular arrangement of the *axial-shear* coupling moduli in the matrix representation of the micropolar elastic tensor relating stress and strain of the homogenized material.

The nonlocal elastic energy density at $\mathbf{x}$, namely the macroelastic energy density (Silling and Askari, 2005), is obtained by integrating the pairwise potential $\mathrm{w}(\mathbf{x}, \mathbf{x}', t)$ over the horizon region $H_\mathbf{x}$ of radius δ

$$\mathcal{W}(\mathbf{x}, t) = \frac{1}{2} \int_{H_\mathbf{x}} \mathrm{w}(\mathbf{x}, \mathbf{x}', t) \, \mathrm{d}\mathbf{x}' \tag{8}$$

The Hamiltonian action integral is defined as

$$\mathcal{H} = \int_{t_1}^{t_2} \int_\Omega \left\{ \mathcal{E}(\mathbf{x}, t) + \mathcal{V}(\mathbf{x}, t) - \mathcal{W}(\mathbf{x}, t) \right\} \mathrm{d}\mathbf{x} \, \mathrm{d}t \tag{9}$$

where the density of kinetic energy[1] is

$$\mathcal{E}(\mathbf{x}, t) = \frac{1}{2} \rho \, \dot{\mathbf{u}} \cdot \dot{\mathbf{u}} + \frac{1}{2} \varrho \, \dot{\theta}^2 \tag{10}$$

while the virtual work of the assigned body forces and couples is

$$\mathcal{V}(\mathbf{x}, t) = \boldsymbol{b} \cdot \mathbf{u} + c \, \theta \tag{11}$$

By substituting the latter relation together with Eqs. (8),(10) in Eq. (9), considering Eqs. (1)–(3), and imposing the stationarity of the functional $\mathcal{H}$, we obtain

$$\delta \mathcal{H} = \int_{t_1}^{t_2} \int_\Omega \left\{ (\boldsymbol{b} \cdot \delta \mathbf{u} + c \, \delta \theta) + \int_{H_\mathbf{x}} \Lambda \left[k_\mathrm{n} \frac{\boldsymbol{\eta} \cdot \mathbf{n}}{\|\boldsymbol{\xi}\|} \delta \mathbf{u} \cdot \mathbf{n} \right.\right.$$
$$+ k_\mathrm{a} \left(\frac{\boldsymbol{\eta} \cdot \mathbf{t}}{\|\boldsymbol{\xi}\|} - \bar{\theta} \right) \delta \mathbf{u} \cdot \mathbf{n} + k_\mathrm{t} \left(\frac{\boldsymbol{\eta} \cdot \mathbf{t}}{\|\boldsymbol{\xi}\|} - \bar{\theta} \right) \delta \mathbf{u} \cdot \mathbf{t}$$
$$+ k_\mathrm{a} \frac{\boldsymbol{\eta} \cdot \mathbf{n}}{\|\boldsymbol{\xi}\|} \delta \mathbf{u} \cdot \mathbf{t} + \frac{k_\mathrm{t}}{2} \left(\frac{\boldsymbol{\eta} \cdot \mathbf{t}}{\|\boldsymbol{\xi}\|} - \bar{\theta} \right) \|\boldsymbol{\xi}\| \delta \theta + k_\mathrm{a} \frac{\boldsymbol{\eta} \cdot \mathbf{n}}{2} \delta \theta + k_\mathrm{b} \frac{\vartheta}{\|\boldsymbol{\xi}\|} \delta \theta \right] \mathrm{d}\mathbf{x}' +$$
$$\left. - \left(\rho \, \ddot{\mathbf{u}} \cdot \delta \mathbf{u} + \varrho \, \ddot{\theta} \, \delta \theta \right) \right\} \mathrm{d}\mathbf{x} \, \mathrm{d}t = 0 \tag{12}$$

where δ denotes the mathematical symbol for variation (Diana et al., 2022). Eq. (12) allows deriving the field equations at $\mathbf{x} \in \Omega$

$$\int_{H_\mathbf{x}} \mathbf{f}(\mathbf{u}', \mathbf{u}, \theta', \theta, \mathbf{x}', \mathbf{x}) \mathrm{d}\mathbf{x}' + \boldsymbol{b}(\mathbf{x}, t) = \rho \ddot{\mathbf{u}}(\mathbf{x}, t) \tag{13}$$

$$\int_{H_\mathbf{x}} \mathrm{m}(\mathbf{u}', \mathbf{u}, \theta', \theta, \mathbf{x}', \mathbf{x}) \mathrm{d}\mathbf{x}' + c(\mathbf{x}, t) = \varrho \ddot{\theta}(\mathbf{x}, t) \tag{14}$$

---

[1] Non-local inertiae can be also included in the mathematical formulation, especially for reproducing the intrinsic dynamic properties of microstructured materials in the regime of short and medium wavelengths (Bacigalupo and Gambarotta, 2017; Diana et al., 2023).

where $\mathbf{f}(\mathbf{u}', \mathbf{u}, \theta', \theta, \mathbf{x}', \mathbf{x}) = \mathbf{f}(\boldsymbol{\eta}, \theta', \theta, \mathbf{x}', \mathbf{x})$ is the force density vector function given by

$$\mathbf{f}(\boldsymbol{\eta}, \theta', \theta, \mathbf{x}', \mathbf{x}) = \Lambda \left[k_\mathrm{n} \frac{\boldsymbol{\eta} \cdot \mathbf{n}}{\|\boldsymbol{\xi}\|} \mathbf{n} + k_\mathrm{a} \left(\frac{\boldsymbol{\eta} \cdot \mathbf{t}}{\|\boldsymbol{\xi}\|} - \frac{\theta' + \theta}{2} \right) \mathbf{n} \right.$$
$$\left. + k_\mathrm{t} \left(\frac{\boldsymbol{\eta} \cdot \mathbf{t}}{\|\boldsymbol{\xi}\|} - \frac{\theta' + \theta}{2} \right) \mathbf{t} + k_\mathrm{a} \frac{\boldsymbol{\eta} \cdot \mathbf{n}}{\|\boldsymbol{\xi}\|} \mathbf{t} \right] \tag{15}$$

and $\mathrm{m}(\mathbf{u}', \mathbf{u}, \theta', \theta, \mathbf{x}', \mathbf{x}) = \mathrm{m}(\boldsymbol{\eta}, \theta', \theta, \mathbf{x}', \mathbf{x})$ is the moment density function given by

$$\mathrm{m}(\boldsymbol{\eta}, \theta', \theta, \mathbf{x}', \mathbf{x}) = \Lambda \left[\frac{k_\mathrm{t}}{2} \left(\frac{\boldsymbol{\eta} \cdot \mathbf{t}}{\|\boldsymbol{\xi}\|} - \frac{\theta' + \theta}{2} \right) \|\boldsymbol{\xi}\| + k_\mathrm{a} \frac{\boldsymbol{\eta} \cdot \mathbf{n}}{2} + k_\mathrm{b} \frac{\theta' - \theta}{\|\boldsymbol{\xi}\|} \right] = \mathrm{m}_\mathrm{t} + \mathrm{m}_\mathrm{b} \tag{16}$$

As it will be shown later in detail, when considering the special case of CM model for standard elasticity, the micromoduli functions k_a and k_b turn out to be analytically vanishing, and the balance equations can then be rewritten in terms of microforces only (Diana, 2023). This result is consistent with Voigt (1928).

A meshfree scheme is considered in this work for the spatial discretization of the CM governing equations (Silling and Askari, 2005; Diana, 2023). The analytical scheme and the variational procedure used to derive the discretized algebraic system of equations referred to the generic solid body occupying a closed domain Ω is detailed in Appendix.

2.1. Material properties and micropotential functions

Given the reference orthonormal basis $\{\mathbf{e}_1, \mathbf{e}_2\}$ defined in Section 2, the general form of the uncoupled constitutive relations of bi-dimensional centrosymmetric micropolar continua can be written in compact matrix Voigt notation as

$$\boldsymbol{\sigma} = \mathbf{C}\boldsymbol{\varepsilon}$$
$$\boldsymbol{\varsigma} = \mathbf{E}\boldsymbol{\varkappa} \tag{17}$$

which in component form read

$$\begin{Bmatrix} \sigma_{11} \\ \sigma_{22} \\ \sigma_{12} \\ \sigma_{21} \end{Bmatrix} = \begin{bmatrix} C_{1111} & C_{1122} & C_{1112} & C_{1121} \\ C_{1122} & C_{2222} & C_{2212} & C_{2221} \\ C_{1112} & C_{2212} & C_{1212} & C_{1221} \\ C_{1121} & C_{2221} & C_{1221} & C_{2121} \end{bmatrix} \begin{Bmatrix} \varepsilon_{11} \\ \varepsilon_{22} \\ \varepsilon_{12} \\ \varepsilon_{21} \end{Bmatrix} \tag{18}$$

$$\begin{Bmatrix} \varsigma_{31} \\ \varsigma_{32} \end{Bmatrix} = \begin{bmatrix} E_{3131} & E_{3132} \\ E_{3132} & E_{3232} \end{bmatrix} \begin{Bmatrix} \varkappa_{31} \\ \varkappa_{32} \end{Bmatrix} \tag{19}$$

the strain tensor components being $\varepsilon_{ih} = \mathrm{u}_{i,h} + \epsilon_{3ih}\phi_3$ with u_i displacement field and $\phi_3 = \phi$ micro-rotation field, while $\varkappa_{3i} = \phi_{3,i}$. The stress tensor and couple-stress vector components are instead denoted by σ_{ih} and ς_{3i}, respectively. The components of the fourth-order elasticity tensor $\mathbb{C} = C_{ihjl}\mathbf{e}_i \otimes \mathbf{e}_h \otimes \mathbf{e}_j \otimes \mathbf{e}_l$ are C_{ihjl}, whereas E_{3i3h} are the components of the equivalent reduced second-order tensor relating the curvature vector $\boldsymbol{\varkappa}$ and the couple-stress vector $\boldsymbol{\varsigma}$.

Considering now a generic orthogonal basis $\{\hat{\mathbf{e}}_1, \hat{\mathbf{e}}_2\}$, obtained from rigid rotation of the reference basis, Eqs. (17) can be rewritten as

$$\hat{\boldsymbol{\sigma}} = \hat{\mathbf{C}}\hat{\boldsymbol{\varepsilon}}$$
$$\hat{\boldsymbol{\varsigma}} = \hat{\mathbf{E}}\hat{\boldsymbol{\varkappa}} \tag{20}$$

where $\hat{\boldsymbol{\sigma}} = \mathbf{Q}_S^\top \boldsymbol{\sigma}$, $\hat{\boldsymbol{\varepsilon}} = \mathbf{Q}_S^\top \boldsymbol{\varepsilon}$, $\hat{\boldsymbol{\varsigma}} = \mathbf{Q}^\top \boldsymbol{\varsigma}$ and $\hat{\boldsymbol{\varkappa}} = \mathbf{Q}^\top \boldsymbol{\varkappa}$, with

$$\mathbf{Q}_S = \begin{bmatrix} \cos^2 \psi & \sin^2 \psi & -\sin \psi \cos \psi & -\sin \psi \cos \psi \\ \sin^2 \psi & \cos^2 \psi & \sin \psi \cos \psi & \sin \psi \cos \psi \\ \sin \psi \cos \psi & -\sin \psi \cos \psi & \cos^2 \psi & -\sin^2 \psi \\ \sin \psi \cos \psi & -\sin \psi \cos \psi & -\sin^2 \psi & \cos^2 \psi \end{bmatrix} \tag{21}$$

and

$$\mathbf{Q} = \begin{bmatrix} \cos\psi & -\sin\psi \\ \sin\psi & \cos\psi \end{bmatrix} \tag{22}$$

respectively. Note that $\mathbf{Q}_S$ is associated with $\mathbf{Q}$, which is a proper orthogonal tensor ($\det\mathbf{Q} = 1$). The angle $\psi = \mathrm{Arg}\left(\hat{\mathbf{e}}_1 \cdot \mathbf{e}_1 + \imath\hat{\mathbf{e}}_1 \cdot \mathbf{e}_2\right)$ is positive if the basis rotation is counterclockwise, with $\hat{\mathbf{C}}$ and $\hat{\mathbf{E}}$ in Eqs. (21)–(22) being defined as

$$\hat{\mathbf{C}} = \begin{bmatrix} \hat{C}_{1111} & \hat{C}_{1122} & \hat{C}_{1112} & \hat{C}_{1121} \\ \hat{C}_{1122} & \hat{C}_{2222} & \hat{C}_{2212} & \hat{C}_{2221} \\ \hat{C}_{1112} & \hat{C}_{2212} & \hat{C}_{1212} & \hat{C}_{1221} \\ \hat{C}_{1121} & \hat{C}_{2221} & \hat{C}_{1221} & \hat{C}_{2121} \end{bmatrix} = \mathbf{Q}_S^\top \mathbf{C} \mathbf{Q}_S \tag{23}$$

$$\hat{\mathbf{E}} = \begin{bmatrix} \hat{E}_{3131} & \hat{E}_{3132} \\ \hat{E}_{3132} & \hat{E}_{3232} \end{bmatrix} = \mathbf{Q}^\top \mathbf{E} \mathbf{Q} \tag{24}$$

According to Eqs. (23)–(24), the off-axis moduli $\hat{C}_{ihjl}$ with $i, h, j, l = 1, 2$ and $\hat{E}_{3i3h}$ with $i, h = 1, 2$ can be written as circular functions of the angle ψ as

$$\hat{C}_{ihjl} = \hat{C}_{ihjl}(\psi) = \hat{C}_{ihjl}(\psi, C_{ihjl})$$
$$\hat{E}_{3i3h} = \hat{E}_{3i3h}(\psi) = \hat{E}_{3i3h}(\psi, E_{3i3h}) \tag{25}$$

where C_{ihjl} and E_{3i3h} are the given elastic constants defining the centrosymmetric in-plane fully anisotropic Cosserat elasticity.[2] Mirror reflection operations (across a line at an angle of $\tilde{\psi} = \psi/2$) is instead defined for the elastic matrix $\mathbf{C}$ and non-local elastic matrix[3] $\mathbf{E}$ by substituting $\mathbf{Q}_S$ and $\mathbf{Q}$ in Eqs. (23)–(24) with

$$\mathbf{Q}_S^\vert = \begin{bmatrix} \cos^2\psi & \sin^2\psi & \sin\psi\cos\psi & \sin\psi\cos\psi \\ \sin^2\psi & \cos^2\psi & -\sin\psi\cos\psi & -\sin\psi\cos\psi \\ \sin\psi\cos\psi & -\sin\psi\cos\psi & -\cos^2\psi & \sin^2\psi \\ \sin\psi\cos\psi & -\sin\psi\cos\psi & \sin^2\psi & -\cos^2\psi \end{bmatrix} \tag{26}$$

and

$$\mathbf{Q}^\vert = \begin{bmatrix} \cos\psi & \sin\psi \\ \sin\psi & -\cos\psi \end{bmatrix} \tag{27}$$

Hence, considering that a reflection matrix is symmetric as well as orthogonal, Eqs. (23)–(24) can be rewritten as

$$\tilde{\mathbf{C}} = \tilde{\tilde{\mathbf{C}}} = \begin{bmatrix} \tilde{C}_{1111} & \tilde{C}_{1122} & \tilde{C}_{1112} & \tilde{C}_{1121} \\ \tilde{C}_{1122} & \tilde{C}_{2222} & \tilde{C}_{2212} & \tilde{C}_{2221} \\ \tilde{C}_{1112} & \tilde{C}_{2212} & \tilde{C}_{1212} & \tilde{C}_{1221} \\ \tilde{C}_{1121} & \tilde{C}_{2221} & \tilde{C}_{1221} & \tilde{C}_{2121} \end{bmatrix} = \mathbf{Q}_S^\vert \mathbf{C} \mathbf{Q}_S^\vert \tag{28}$$

$$\tilde{\mathbf{E}} = \tilde{\tilde{\mathbf{E}}} = \begin{bmatrix} \tilde{E}_{3131} & \tilde{E}_{3132} \\ \tilde{E}_{3132} & \tilde{E}_{3232} \end{bmatrix} = \mathbf{Q}^\vert \mathbf{E} \mathbf{Q}^\vert \tag{29}$$

from which it follows that in this case, given an orthonormal basis, the material reflection operation is equivalent to the reflection operation applied to the orthonormal basis, with the material configuration being unchanged (the transformed mathematical objects are denoted by $\tilde{\mathbf{C}}$ and $\tilde{\tilde{\mathbf{E}}}$ in the former case). Note that $\mathbf{Q}_S^\vert$ is associated with $\mathbf{Q}^\vert$, which is an improper orthogonal tensor ($\det\mathbf{Q}^\vert = -1$). By applying the reflection operator to the elastic matrix $\mathbf{C}$ and non-local elastic matrix $\mathbf{E}$ with respect to the directions (e.g. axes) defined by the reference basis unit vectors $\mathbf{e}_1$ and $\mathbf{e}_2$, Eqs. (28)–(29) give the relations

$$\tilde{C}_{iiij} = \tilde{\tilde{C}}_{iiij} = -C_{iiij}, \quad \tilde{C}_{iiji} = \tilde{\tilde{C}}_{iiji} = -C_{iiji} \tag{30}$$

---

[2] In the most general (centrosymmetric) two-dimensional case, the number of independent material constants in Eq. (18) is ten. If not otherwise specified, the attention is focused on orthotropic chiral and achiral materials in generic coordinate description.

[3] It can be shown that both $\mathbf{C}$ and $\mathbf{E}$ transform as true tensors (Desmorat et al., 2023).

with $i, j = 1, 2$ and

$$\tilde{E}_{3132} = \tilde{\tilde{E}}_{3132} = -E_{3132} \tag{31}$$

the other elasticities remaining unchanged after performing the orthogonal operations defined above. More in general, it can be shown that this property holds also for micropolar constitutive matrices written considering a generic basis, if they are reflected with respect to one of the two axes defined by the corresponding basis unit vectors. It follows that, under these conditions, the elastic moduli C_{iiij}, C_{iiji} and E_{3132} show sensitivity to mirror reflection operations of the orthonormal basis (or, alternatively, to material reflection), while the remaining elasticities do not. It is worth to note that this property is related to the anisotropy of the corresponding tensors, as well as to the chiral properties of the material homogenized as a micropolar continuum. Actually, if it characterizes also the rotationally invariant (hemitropic) part of the constitutive tensor[4],[5] the corresponding bi-dimensional micropolar solid (regardless of its elastic anisotropy) turns out to be chiral, as specified in Zou et al. (2001), Chen et al. (2014b). Hence, the orthogonal irreducible decomposition of the elastic tensors (Zou et al., 2001) is proved useful to identify chiral properties owing to SO(2) invariance.

The mechanistic nature of the continuum-molecular model requires the definition of pairwise constitutive laws for microstructure (i.e. the virtual fibers, namely the pairwise interactions) such that the overall elastic behavior of the material is the result of the assigned micro-interactions properties (Diana et al., 2022). Besides, to assign microscopic properties on the basis of macroscopic ones, the identification of a *representative cell* is of the essence (DiCarlo and Podio-Guidugli, 2021; Diana et al., 2022). In non-local models of this kind, the representative cell is the horizon region $H_{\mathbf{x}}$ over the integral in Eq. (8) is defined, while the micro-macro moduli correspondence principle is based on a micro-macro energy equivalence, which allows macroscopic properties to be directly associated to microscale-defined constitutive laws (Diana, 2023). Considering the constitutive behavior of in-plane centrosymmetric micropolar linear elastic media which is defined by ten independent elastic moduli C_{ihjl} together with the uncoupled moduli E_{3i3h}, it can be shown that the micromoduli functions $k_{\mathrm{n}}(\psi)$, $k_{\mathrm{t}}(\psi)$, $k_{\mathrm{a}}(\psi)$ and $k_{\mathrm{b}}(\psi)$ introduced in Section 2 may be written in general form as

$$k_{\mathrm{n}}(\psi) = k_{\mathrm{n}}(\psi, \mathcal{K}_{1111}, \mathcal{K}_{1122}, \mathcal{K}_{2222}, \mathcal{K}_{1112}, \mathcal{K}_{1121}, \mathcal{K}_{2212},$$

---

[4] The micropolar constitutive tensors, expressed in matrix form by $\mathbf{C}$ and $\mathbf{E}$ in Eqs. (17), possess a hierarchical structure and can be decomposed into several parts according to the symmetry of the underlying microstructure (Chen et al., 2014b). The following relations hold

$$\mathbf{C} = \mathbf{C}_o + \mathbf{C}_4 + \mathbf{C}_2$$
$$\mathbf{E} = \mathbf{E}_o + \mathbf{E}_2 \tag{32}$$

where $\mathbf{C}_o$ and $\mathbf{E}_o$ are the rotationally invariant parts of $\mathbf{C}$ and $\mathbf{E}$, respectively, while the remaining terms refer to their anisotropic parts with $\mathbb{D}_4$ invariance (four axes of reflection symmetry) and $\mathbb{D}_2$ invariance (two axes of reflection symmetry), respectively. While $\mathbf{E}_o$ is isotropic (Spencer, 1970), $\mathbf{C}_o$ can show O(2) or SO(2) invariance. In particular, if $\mathbf{C}_o$ is SO(2) invariant, namely hemitropic (invariant, in general, under basis or material rotations but not under mirror reflections), the corresponding micropolar solid turns out to be consequently chiral (Chen et al., 2014a) (for further details refer to Zou et al. (2001), Chen et al. (2014b)). It is noted that for a *chiral orthotropic* solid ($\mathbf{C}_o$ is SO(2) invariant), if the last terms of Eqs. (32) are vanishing, the overall continuum is characterized by $\mathbb{Z}_4$ invariance (i.e. invariance under $n\pi/2$ rotation of coordinate). If not, the principal axes of $\mathbf{C}_2$ are included in and aligned with those of $\mathbf{C}_4$, the micropolar continuum being characterized by overall $\mathbb{Z}_2$ invariance (i.e. invariance under $n\pi$ rotation of coordinate).

[5] The set of symmetry classes in centrosymmetric 2D micropolar elasticity is $\mathfrak{I} = \left\{ [\mathbb{Z}_2], [\mathbb{D}_2], [\mathbb{Z}_4], [\mathbb{D}_4], [\mathrm{SO}(2)], [\mathrm{O}(2)] \right\}$ (Auffray et al., 2022; Trovalusci and Masiani, 1999). The $\mathbb{Z}_2$ class includes *chiral orthotropic* solids (with, in general, non-vanishing $\mathbf{C}_2$ and $\mathbf{E}_2$) as well as fully anisotropic media (which are then also chiral by definition, regardless of $\mathbf{C}_o$). General definitions of $\mathbb{D}_k$ and $\mathbb{Z}_n$ invariance are given in Auffray et al. (2022), Auffray and Ropars (2016), Forte and Vianello (1996).

$$\mathcal{K}_{2221}, \mathcal{K}_{1212}, \mathcal{K}_{1221}, \mathcal{K}_{2121}) \tag{33}$$

$$k_{\mathrm{t}}(\psi) = k_{\mathrm{t}}(\psi, \mathcal{K}_{1111}, \mathcal{K}_{1122}, \mathcal{K}_{2222}, \mathcal{K}_{1112}, \mathcal{K}_{1121}, \mathcal{K}_{2212},$$

$$\mathcal{K}_{2221}, \mathcal{K}_{1212}, \mathcal{K}_{1221}, \mathcal{K}_{2121}) \tag{34}$$

$$k_{\mathrm{a}}(\psi) = k_{\mathrm{a}}(\psi, \mathcal{K}_{1112}, \mathcal{K}_{1121}, \mathcal{K}_{2212}, \mathcal{K}_{2221}) \tag{35}$$

$$k_{\mathrm{b}}(\psi) = k_{\mathrm{b}}(\psi, \mathcal{K}_{3131}, \mathcal{K}_{3132}, \mathcal{K}_{3232}) \tag{36}$$

where $\mathcal{K}_{ihjl}$ with $i, h, j, l = 1, 2$ and $\mathcal{K}_{3i3h}$ with $i, h = 1, 2$ are the material micromoduli characterizing the continuum-molecular model for two-dimensional micropolar elasticity. They define the polar microelastic functions and then the directional dependency of the pairwise constitutive laws of virtual fibers (Diana, 2023). It is worth to note that the set of (analytical) micropotential functions (Eqs. (33)–(36)) capable to reproduce the overall elastic behavior of a micropolar solid characterized by a given anisotropic structure is not unique (Diana, 2023).

Let us assume here, without losing generality and in analogy with the micropolar continuum[6] (Cosserat and Cosserat, 1909), that the pairwise axial, shear and bending micromoduli functions $k_{\mathrm{n}}(\psi)$, $k_{\mathrm{t}}(\psi)$ and $k_{\mathrm{b}}(\psi)$ exhibit a directional dependency as $\hat{C}_{1111}(\psi)$, $\hat{C}_{2121}(\psi)$ and $\hat{E}_{3131}(\psi)$ in Eqs. (23) and (24), respectively. Hence,

$$
\begin{aligned}
k_{\mathrm{n}}(\psi) = &\mathcal{K}_{1111} \cos^4 \psi + 2\left(\mathcal{K}_{1112} + \mathcal{K}_{1121}\right) \sin \psi \cos^3 \psi \\
&+ \left(2\mathcal{K}_{1122} + \mathcal{K}_{1212} + 2\mathcal{K}_{1221} + \mathcal{K}_{2121}\right) \sin^2 \psi \cos^2 \psi \\
&+ 2 \sin^3 \psi \cos \psi \left(\mathcal{K}_{2221} + \mathcal{K}_{2212}\right) + \mathcal{K}_{2222} \sin^4 \psi
\end{aligned} \tag{37}
$$

$$
\begin{aligned}
k_{\mathrm{t}}(\psi) = &\mathcal{K}_{2121} \cos^4 \psi + 2\left(\mathcal{K}_{2221} - \mathcal{K}_{1121}\right) \sin \psi \cos^3 \psi \\
&+ \left(\mathcal{K}_{1111} + \mathcal{K}_{2222} - 2\mathcal{K}_{1122} - 2\mathcal{K}_{1221}\right) \sin^2 \psi \cos^2 \psi \\
&+ 2 \sin^3 \psi \cos \psi \left(\mathcal{K}_{1112} - \mathcal{K}_{2212}\right) + \mathcal{K}_{1212} \sin^4 \psi
\end{aligned} \tag{38}
$$

$$k_{\mathrm{b}}(\psi) = \mathcal{K}_{3131} \cos^2 \psi + 2\mathcal{K}_{3132} \sin \psi \cos \psi + \mathcal{K}_{3232} \sin^2 \psi \tag{39}$$

where $\mathcal{K}_{1111}$ and $\mathcal{K}_{2222}$ are the microelastic axial moduli of virtual fibers parallel to the unit vectors $\mathbf{e}_1$ and $\mathbf{e}_2$, respectively, whereas $\mathcal{K}_{2121}$ and $\mathcal{K}_{1212}$ are the microelastic shear moduli corresponding to virtual fibers along the directions defined by the aforementioned unit vectors. Differently, $\mathcal{K}_{1122}$ and $\mathcal{K}_{1221}$ are axial-axial and shear-shear coupling moduli. Moreover $\mathcal{K}_{1112}$, $\mathcal{K}_{1121}$, $\mathcal{K}_{2212}$ and $\mathcal{K}_{2221}$ are microelastic moduli related to the macro axial-shear couplings in micropolar (Cosserat) anisotropic elasticity. Finally, $\mathcal{K}_{3131}$ and $\mathcal{K}_{3232}$ are the two bending micromoduli referred, as usual, to the orthogonal directions defined by $\mathbf{e}_1$ and $\mathbf{e}_2$, respectively, while $\mathcal{K}_{3132}$ is a bending-bending coupling micromodulus[7].

It is worth to note that the directional dependent micromoduli in Eqs. (37)–(38) alone are able to describe general coupling between

---

[6] Considering for the generic virtual fiber $\hat{\mathbf{n}} \equiv \hat{\mathbf{e}}_1$, and $\hat{\mathbf{t}} \equiv \hat{\mathbf{e}}_2$.

[7] Eqs. (37)–(39) can be also recast in the equivalent form

$$
\begin{aligned}
k_{\mathrm{n}}(\psi) = \frac{1}{8} \Big[&\mathcal{K}_{1111}(3 + 4 \cdot \cos 2\psi + \cos 4\psi) \\
&+ (\mathcal{K}_{1212} + \mathcal{K}_{2121} + 2\mathcal{K}_{1122} + 2\mathcal{K}_{1221})(1 - \cos 4\psi) \\
&+ 2(\mathcal{K}_{1112} + \mathcal{K}_{1121})(2 \sin 2\psi + \sin 4\psi) \\
&+ 2(\mathcal{K}_{2212} + \mathcal{K}_{2221})(2 \sin 2\psi - \sin 4\psi) \\
&+ \mathcal{K}_{2222}(3 - 4 \cos 2\psi + \cos 4\psi) \Big]
\end{aligned} \tag{40}
$$

$$
\begin{aligned}
k_{\mathrm{t}}(\psi) = \frac{1}{8} \Big[&\mathcal{K}_{2121}(3 + 4 \cdot \cos 2\psi + \cos 4\psi) \\
&+ (\mathcal{K}_{1111} + \mathcal{K}_{2222} - 2\mathcal{K}_{1122} - 2\mathcal{K}_{1221})(1 - \cos 4\psi) \\
&+ 2(\mathcal{K}_{1112} - \mathcal{K}_{2212})(2 \sin 2\psi - \sin 4\psi) \\
&+ 2(\mathcal{K}_{2221} - \mathcal{K}_{1121})(2 \sin 2\psi + \sin 4\psi) \\
&+ \mathcal{K}_{1212}(3 - 4 \cos 2\psi + \cos 4\psi) \Big]
\end{aligned} \tag{41}
$$

$$k_{\mathrm{b}}(\psi) = \frac{1}{2}\left[\mathcal{K}_{3131}(1 + \cos 2\psi) + \mathcal{K}_{3232}(1 - \cos 2\psi) + 2\mathcal{K}_{3132} \sin 2\psi \right] \tag{42}$$

which may be useful for a direct understanding the structure of the micropotential function.

---

macro shear and axial deformation due to directional anisotropy in micropolar solids. Specifically, the micromodulus function $k_{\mathrm{a}}(\psi)$ introduced in Eq. (4), and whose general form is given in Eq. (35), is not required when considering achiral micropolar continua (more in general, when $\mathbf{C}_o$ is O(2) invariant). Actually, the presence of the additional pair potential term $k_{\mathrm{a}}(\psi)$ in Eq. (4) is related to that of a hemitropic part of $\mathbf{C}$ with SO(2) invariance (Chen et al., 2014b). The directional-independent function

$$k_{\mathrm{a}}(\psi) = k_{\mathrm{a}} = \Gamma \left[(\mathcal{K}_{2221} - \mathcal{K}_{2212}) + (\mathcal{K}_{1121} - \mathcal{K}_{1112}) \right] \tag{43}$$

is defined, having the formal structure of the scalar-valued directional-independent variable

$$C_{\mathscr{H}} = \Gamma \{[C_{2221} - C_{2212}] + [C_{1121} - C_{1112}]\} \tag{44}$$

with $\Gamma \in \mathbb{N}^+$ ($\Gamma = 1/2$ is considered here for convenience). Actually, for any given rotation defined by the angle ψ, Eqs. (23) and (44) lead to the relation

$$[(\hat{C}_{2221} - \hat{C}_{2212}) + (\hat{C}_{1121} - \hat{C}_{1112})] = [(C_{2221} - C_{2212}) + (C_{1121} - C_{1112})] \tag{45}$$

Considering instead reflection symmetry operations across any arbitrary line defined by the angle $\tilde{\psi} = \psi/2$, from Eq. (29) and Eq. (44) we obtain

$$[(\tilde{C}_{2221} - \tilde{C}_{2212}) + (\tilde{C}_{1121} - \tilde{C}_{1112})] = -[(C_{2221} - C_{2212}) + (C_{1121} - C_{1112})] \tag{46}$$

Hence, $C_{\mathscr{H}}$ is a pseudo-scalar which has the property to be invariant under arbitrary basis (or material) rotations, while inverting its sign for arbitrary mirror reflections operations as defined above. Consequently, $C_{\mathscr{H}}$ turns out to be non-vanishing in the case that the rotationally invariant part of the micropolar elastic tensor is rather not invariant to mirror reflections, its sign being dependent on the handedness of the microstructure. By invoking the orthogonal irreducible decomposition of elastic tensors (Zou et al., 2001), it is easy to show that $C_{\mathscr{H}}$ is function through Γ of the chiral elastic constant A characterizing the hemitropic part of $\mathbf{C}$ (see Section 3). The micromodulus constant function k_{a} allows then modeling those couplings behaviors uncovered by Eqs. (37)–(38) and specific of centrosymmetric micropolar periodic microstructures with chiral topology. Actually, if the hemitropic part of $\mathbf{C}$ is not isotropic as well, $C_{\mathscr{H}}$ results to be non-vanishing regardless of the symmetry class (SO(2), $\mathbb{Z}_4$, i.e. invariance under $n\pi/2$ rotation of coordinate, or $\mathbb{Z}_2$, i.e. invariance under $n\pi$ rotation of coordinate) of the overall constitutive tensor. As it will be shown later, since the properties exhibited by $C_{\mathscr{H}}$ naturally hold for k_{a} as well, a properly defined mirror reflection operation of the elastic matrix $\mathbf{C}$ characterizing a given chiral micropolar continuum, results in a sign inversion of the pseudo-scalar micropotential term in Eq. (43), which thus provides the information of chirality owing to SO(2) invariance in the CM model. Moreover, it is apparent from the considerations above that k_{a} turns out, naturally and analytically, to be vanishing for all achiral micropolar solids with arbitrary orientation of the material reference system (e.g. micropolar media with $\mathbb{D}_2$, $\mathbb{D}_4$ and O(2) invariance). In these cases, (as well as in the other cases of asymmetry not explicitly mentioned here), material anisotropy and related couplings behaviors can be fully represented by the directional dependent axial and shear micropotential functions in Eqs. (37)–(38) (see also Diana (2023)). Finally it can be noted that the effective anisotropy of $\mathbf{E}$ can be fully represented (in a mechanism-based framework) by the micropotential function in Eq. (39), even in the most general case of chiral solids with $\mathbb{Z}_2$ invariance[8] (i.e. the elastic tensor is invariant under $n\pi$ rotation of coordinates), E_{3132} being a constant related to classical anisotropy, not to chirality (Chen et al., 2014b). This because axes of reflection symmetry always exist for $\mathbf{E}$. Interestingly, as for global anisotropy, the effective coupling between bulk strain and micro-rotation, which may

---

[8] $\hat{E}_{3131}(\psi)$, as well as $\hat{C}_{1111}(\psi)$ and $\hat{C}_{2121}(\psi)$, assume the same formal structure of $\tilde{E}_{3131}(\psi)$, $\tilde{C}_{1111}(\psi)$ and $\tilde{C}_{2121}(\psi)$, respectively.

be observed in micropolar chiral solids (Chen et al., 2014b; Giorgio et al., 2020), can be fully reproduced by the definition of proper pairwise micro-constitutive relation.

In the following subsection, we establish analytical relations between the aforementioned microelastic moduli and the corresponding elasticities of a centrosymmetric two-dimensional micropolar Cosserat continuum, adopting a general and consistent approach that does not require the definition of specific deformation fields.

2.1.1. Micro-macro moduli identification

Let us consider a time-independent two-dimensional deformation field. The components of ε and $\varkappa$ are assumed, without loss of generality, not to depend on the specific position $\mathbf{x} \in \Omega$. The elastic energy density of a two-dimensional centrosymmetric micropolar continuum reads

$$\begin{aligned}
\varphi_{\mathscr{C}} + \varphi_{\mathscr{E}} = \frac{1}{2} \Big[& (C_{1111}\varepsilon_{11}^2 + C_{2222}\varepsilon_{22}^2 + 2C_{1122}\varepsilon_{11}\varepsilon_{22} \\
& + C_{1212}\varepsilon_{12}^2 + C_{2121}\varepsilon_{21}^2 + 2C_{1221}\varepsilon_{12}\varepsilon_{21} \\
& + 2C_{1112}\varepsilon_{11}\varepsilon_{12} + 2C_{1121}\varepsilon_{11}\varepsilon_{21} + 2C_{2212}\varepsilon_{22}\varepsilon_{12} + 2C_{2221}\varepsilon_{22}\varepsilon_{21}) \\
& + (E_{3131}\varkappa_{31}^2 + 2E_{3132}\varkappa_{31}\varkappa_{32} + E_{3232}\varkappa_{32}^2) \Big]
\end{aligned} \tag{47}$$

where the elasticities and the macro-strain and curvatures components are defined in the reference basis $\{\mathbf{e}_1, \mathbf{e}_2\}$. According to Eq. (8) and Eqs. (37)–(43), the corresponding quantity for the continuum-molecular model is instead given by the general integral

$$\begin{aligned}
\mathcal{W} = \frac{1}{2} \int_{H_{\mathbf{X}}} & [w_s(\mathbf{x}, \mathbf{x}') + w_\gamma(\mathbf{x}, \mathbf{x}') + w_{s\gamma}(\mathbf{x}, \mathbf{x}') + w_\chi(\mathbf{x}, \mathbf{x}')] \, d\mathbf{x}' \\
= \frac{h}{4} \int_0^\delta & \left\{ \|\xi\|^2 \Lambda(\|\xi\|) \int_0^{2\pi} \left[k_n(\psi)s^2(\psi) + k_t(\psi)\gamma^2(\psi) \right. \right. \\
& \left. \left. + k_a s(\psi)\gamma(\psi) + k_b(\psi)\chi^2(\psi) \right] d\psi \right\} d\|\xi\|
\end{aligned} \tag{48}$$

where, under the assumed conditions, the pairwise deformations $s(\psi)$, $\gamma(\psi)$ and $\chi(\psi)$ of the generic virtual fiber can be expressed as linear functions of the macro-strain ε_{ih} and curvature $\varkappa_{3i}$ components, and as quadratic functions of the direction cosines of the orthonormal unit vectors $\mathbf{n} = n_i\mathbf{e}_i$ and $\mathbf{t} = t_i\mathbf{e}_i$ by

$$s(\psi) = \hat{\varepsilon}_{11}(\psi) = \varepsilon_{nn}(\psi) = \varepsilon_{ij}n_i n_j \tag{49}$$

$$\gamma(\psi) = \hat{\varepsilon}_{21}(\psi) = \varepsilon_{tn}(\psi) = \varepsilon_{ij}t_i n_j \tag{50}$$

$$\chi(\psi) = \hat{\varkappa}_{31}(\psi) = \varkappa_{3n}(\psi) = \varkappa_{3i}n_i \tag{51}$$

which are consistent with the Cauchy-Born rule (Ericksen, 1984, 2008) adapted and generalized to our case, and according to $\hat{\varepsilon} = \mathbf{Q}_S^\top \varepsilon$ and $\hat{\varkappa} = \mathbf{Q}^\top \varkappa$, with $\mathbf{Q}_S$ and $\mathbf{Q}$ being defined by Eqs. (21)–(22), respectively. Hence, the following relations hold

$$s(\psi) = \varepsilon_{11}\cos^2\psi + \varepsilon_{22}\sin^2\psi + (\varepsilon_{12} + \varepsilon_{21})\cos\psi \, \sin\psi \tag{52}$$

$$\gamma(\psi) = \varepsilon_{21}\cos^2\psi - \varepsilon_{12}\sin^2\psi - (\varepsilon_{11} - \varepsilon_{22})\cos\psi \, \sin\psi \tag{53}$$

$$\chi(\psi) = \varkappa_{31}\cos\psi + \varkappa_{32}\sin\psi \tag{54}$$

Substituting Eqs. (52)–(54) in Eq. (48), and assuming $k_n(\psi)$, $k_a(\psi)$, $k_t(\psi)$ and $k_b(\psi)$ by Eqs. (37)–(39), Eq. (48) gives as general solution

$$\begin{aligned}
\mathcal{W} = h\mathcal{N} \Big[& \mathscr{A}_{1111}\varepsilon_{11}^2 + \mathscr{A}_{2222}\varepsilon_{22}^2 + \mathscr{A}_{1122}\varepsilon_{11}\varepsilon_{22} \\
& + \mathscr{A}_{1212}\varepsilon_{12}^2 + \mathscr{A}_{2121}\varepsilon_{21}^2 + \mathscr{A}_{1221}\varepsilon_{12}\varepsilon_{21} + \mathscr{A}_{1112}\varepsilon_{11}\varepsilon_{12} \\
& + \mathscr{A}_{1121}\varepsilon_{11}\varepsilon_{21} + \mathscr{A}_{2212}\varepsilon_{22}\varepsilon_{12} + \mathscr{A}_{2221}\varepsilon_{22}\varepsilon_{21} \\
& + \mathscr{B}_{3131}\varkappa_{31}^2 + \mathscr{B}_{3232}\varkappa_{32}^2 + \mathscr{B}_{3132}\varkappa_{31}\varkappa_{32} \Big]
\end{aligned} \tag{55}$$

where $\mathcal{N} = \mathcal{N}(\delta)$ is a scalar-valued function of the horizon δ, depending on the specific influence function considered while $\mathscr{A}_{ihjl}$ with $i, h, j, l = 1, 2$ and $\mathscr{B}_{3i3h}$ with $i, h = 1, 2$ are functions of the previously defined micromoduli $\mathcal{K}_{ihjl}$ and $\mathcal{K}_{3i3h}$, respectively. In case of dimensionless attenuation functions, $\mathcal{N}$ can be expressed as $\mathcal{N} = \delta^3 \mathcal{Q}$, with $\mathcal{Q} \in \mathbb{R}^+$. In what follows, we assume without loss of generality that $\Lambda(\|\xi\|) = 1$,

thus $\mathcal{Q} = \pi/384$. Hence, comparing Eqs. (47) and (55), and collecting the terms that multiply the same strain ε_{ij} and microcurvature $\varkappa_{3i}$ components, the analytical expressions relating Cosserat macromoduli and continuum-molecular micromoduli are obtained

$$C_{1111} = C\mathscr{A}_{1111}$$
$$= C(19\mathcal{K}_{1111} + 3\mathcal{K}_{2222} + 2\mathcal{K}_{1122} + 5\mathcal{K}_{1212} + 5\mathcal{K}_{2121} + 2\mathcal{K}_{1221})$$
$$C_{2222} = C\mathscr{A}_{2222}$$
$$= C(3\mathcal{K}_{1111} + 19\mathcal{K}_{2222} + 2\mathcal{K}_{1122} + 5\mathcal{K}_{1212} + 5\mathcal{K}_{2121} + 2\mathcal{K}_{1221})$$
$$C_{1122} = C\mathscr{A}_{1122} = C(\mathcal{K}_{1111} + \mathcal{K}_{2222} + 6\mathcal{K}_{1122} + 6\mathcal{K}_{1221} - \mathcal{K}_{1212} - \mathcal{K}_{2121})$$
$$C_{1212} = C\mathscr{A}_{1212}$$
$$= C(5\mathcal{K}_{1111} + 5\mathcal{K}_{2222} - 2\mathcal{K}_{1122} + 19\mathcal{K}_{1212} + 3\mathcal{K}_{2121} - 2\mathcal{K}_{1221})$$
$$C_{2121} = C\mathscr{A}_{2121}$$
$$= C(5\mathcal{K}_{1111} + 5\mathcal{K}_{2222} - 2\mathcal{K}_{1122} + 3\mathcal{K}_{1212} + 19\mathcal{K}_{2121} - 2\mathcal{K}_{1221})$$
$$C_{1221} = C\mathscr{A}_{1221} = C(\mathcal{K}_{1111} + \mathcal{K}_{2222} + 6\mathcal{K}_{1122} + 6\mathcal{K}_{1221} - \mathcal{K}_{1212} - \mathcal{K}_{2121})$$
$$C_{1112} = 2C\mathscr{A}_{1112} = 2C(9\mathcal{K}_{1112} - 3\mathcal{K}_{1121} + 3\mathcal{K}_{2212} - \mathcal{K}_{2221})$$
$$C_{1121} = 2C\mathscr{A}_{1121} = 2C(9\mathcal{K}_{1121} - 3\mathcal{K}_{1112} + 3\mathcal{K}_{2212} - \mathcal{K}_{2221})$$
$$C_{2212} = 2C\mathscr{A}_{2212} = 2C(3\mathcal{K}_{1112} - \mathcal{K}_{1121} + 9\mathcal{K}_{2212} - 3\mathcal{K}_{2221})$$
$$C_{2221} = 2C\mathscr{A}_{2221} = 2C(\mathcal{K}_{1112} - 3\mathcal{K}_{1121} - 3\mathcal{K}_{2212} + 9\mathcal{K}_{2221})$$
$$E_{3131} = 8C\mathscr{B}_{3131} = 8C(3\mathcal{K}_{3131} + \mathcal{K}_{3232})$$
$$E_{3232} = 8C\mathscr{B}_{3232} = 8C(\mathcal{K}_{3131} + 3\mathcal{K}_{3232})$$
$$E_{3132} = 16C\mathscr{B}_{3132} = 16C\mathcal{K}_{3132} \tag{56}$$

where $C = 2h\mathcal{N}$. It is noted that Eqs. (56) lead to the analytical relation $C_{1122} = C_{1221}$. An important consideration is that the obtained relation between axial-axial and shear-shear coupling macromoduli does not depend on the specific micromoduli functions adopted. Moreover, this analytical evidence results to be independent of the attenuation function considered and is rather related to the assumed pair potential description of elasticity under the hypothesis of non-symmetric macro-strain conditions. Similarly to the well known Cauchy relation $C_{1122} = C_{1212}$ (Love, 1944) characterizing mathematical models associated with central pair-potentials for planar standard elasticity (symmetric macro-strains) (Silling, 2000; Love, 1944; Stakgold, 1950; Diana, 2023), the here obtained relation is instead an intrinsic feature of non-central pair potential based formulations for planar micropolar elasticity (non symmetric macro-strains). Another formal similarity with the Cauchy relation is that the aforementioned identity refers, in its irreducible form, to the rotationally invariant part of the elastic tensor of the equivalent continuum, as it is independent of the anisotropy of the material and holds even in case of O(2) invariance. We shall refer to this as *Voigt relation*, in honor to W. Voigt and his pioneering studies on polar elasticity and non-central pair potentials (Voigt, 1887, 1900). It is worth noting that the same relation can be found in chiral or achiral periodic full discrete systems, bi-dimensional block-lattices, and beam-lattices with body(node)-centered periodic cell homogenized as micropolar continua (see Liu et al. (2012), Chen et al. (2014b), Kumar and McDowell (2004), Bacigalupo and Gambarotta (2017, 2020), Casolo (2021) among others), insofar their Lagrangian description can be directly or indirectly associated with the definition of spatially uniform (e.g. not dependent of the specific centroid position) elastic non-central pair-potentials (Diana, 2023). These aspects allow then to establish an interesting natural theoretical correspondence between the continuum-molecular framework and the mechanics of periodic discrete lattice-like materials, which could be of support in the study, the design and the optimization of new architected materials featuring repetitive unit cells composed of rigid elements connected by elastic ligaments or elastic interfaces (Bacigalupo and Gambarotta, 2017; Diana, 2023).

By solving the algebraic system given by Eqs. (56) for the micromoduli, and considering the relations obtained in the reduced case of anisotropic standard elasticity (Diana, 2023), we obtain

$$\mathcal{K}_{1111} = 2\mathcal{Z}(4C_{1111} - 2C_{1221} - C_{1212} - C_{2121}) \tag{57}$$
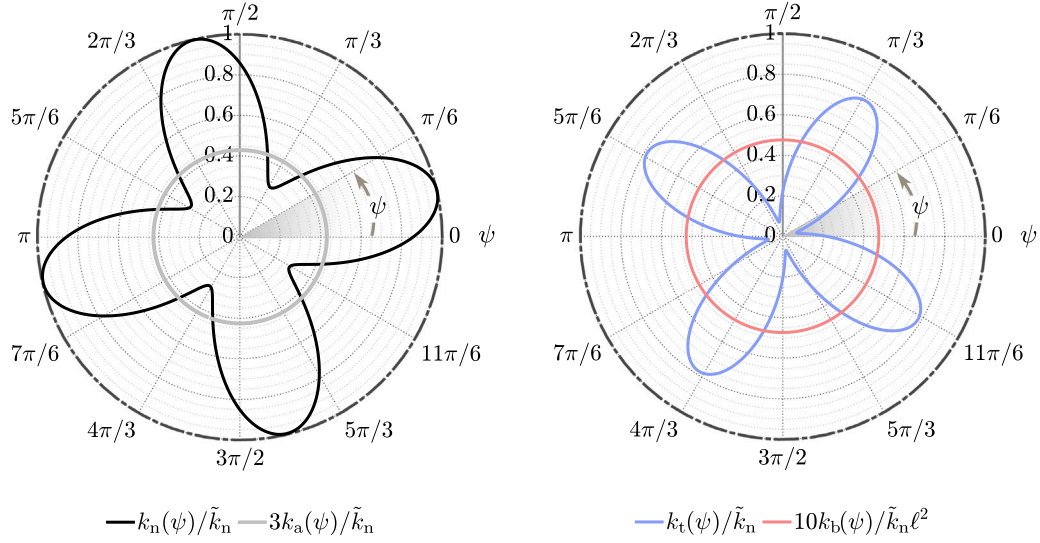
Fig. 2. Polar plots of the normalized micromoduli functions $k_n(\psi)$, $k_t(\psi)$, $k_a(\psi)$ and $k_b(\psi)$ in Eqs. (37)–(43) corresponding to a representative chiral material with $\mathbb{Z}_4$ invariance (block-lattice architectured material with tetrachiral topology whose micropolar continuum elastic tensor is given analytically in Section 3).

$$\mathcal{K}_{2222} = 2\mathscr{Z}(4C_{2222} - 2C_{1221} - C_{1212} - C_{2121}) \tag{58}$$

$$\mathcal{K}_{1122} = 2\mathscr{Z}(12C_{1122} - 2C_{1221} - C_{1212} - C_{2121}) \tag{59}$$

$$\mathcal{K}_{1212} = 2\mathscr{Z}(4C_{1212} + 4C_{1221} - C_{1111} - C_{2222} - 2C_{1122}) \tag{60}$$

$$\mathcal{K}_{2121} = 2\mathscr{Z}(4C_{2121} + 4C_{1221} - C_{1111} - C_{2222} - 2C_{1122}) \tag{61}$$

$$\mathcal{K}_{1221} = 2\mathscr{Z}(2C_{2121} + 2C_{2121} + 4C_{1221} - C_{1111} - C_{2222} - 2C_{1122}) \tag{62}$$

$$\mathcal{K}_{1112} = \mathscr{Z}(9C_{1112} + 3C_{1121} - 3C_{2212} - C_{2221}) \tag{63}$$

$$\mathcal{K}_{1121} = \mathscr{Z}(9C_{1121} + 3C_{1112} - 3C_{2221} - C_{2212}) \tag{64}$$

$$\mathcal{K}_{2212} = \mathscr{Z}(9C_{2212} + 3C_{2221} - 3C_{1112} - C_{1121}) \tag{65}$$

$$\mathcal{K}_{2221} = \mathscr{Z}(9C_{2221} + 3C_{2212} - 3C_{1121} - C_{1112}) \tag{66}$$

$$\mathcal{K}_{3131} = 2\mathscr{Z}(3E_{3131} - E_{3132}) \tag{67}$$

$$\mathcal{K}_{3232} = 2\mathscr{Z}(3E_{3232} - E_{3131}) \tag{68}$$

$$\mathcal{K}_{3132} = 8\mathscr{Z}(E_{3132}) \tag{69}$$

with $\mathscr{Z} = 3/(2\pi h\delta^3)$. It can be noted from Eqs. (57)–(69) that the micromoduli $\mathcal{K}_{1112}$, $\mathcal{K}_{1121}$, $\mathcal{K}_{2212}$, and $\mathcal{K}_{2221}$ in Eqs. (63)–(66) are directly related to the corresponding elasticities C_{1112}, C_{1121}, C_{2212}, and C_{2221}, and that the properties announced for k_a in Eq. (43) turn out to hold analytically. Moreover, consistently with centrosymmetric planar micropolar elasticity, the bending micromoduli turn out to be decoupled with respect to the other micromoduli, these being dependent of the bending macro-moduli E_{3i3h} only. Polar plots of the micromoduli functions $k_n(\psi)$, $k_t(\psi)$, $k_a(\psi)$ and $k_b(\psi)$ in Eqs. (37)–(43) corresponding to a representative chiral material (Bacigalupo and Gambarotta, 2020; Diana et al., 2023) with $\mathbb{Z}_4$ invariance are reported in Fig. 2. Specifically, we refer here to a block-lattice architectured material with tetrachiral topology, for which the micropolar continuum elastic tensor has been identified analytically by Diana et al. (2023). Details about the considered material are reported in Section 3. It should be underlined that under general inhomogeneous deformations, the micropotential functions here detailed fully define the linear elastic macroscopic behavior of the equivalent micropolar continuum (Diana et al., 2022; Diana, 2023), while providing a mechanism-based description of material anisotropy and chirality.

In the special case in which the (structured) material under consideration is homogenized within the framework of standard elasticity (symmetric macro-strains), one obtains $E_{3i3h} = 0$, $C_{1112} = C_{1121}$, $C_{2212} = C_{2221}$ and $C_{1212} = C_{1221} = C_{2121}$. Therefore, Eqs. (57)–(69) reduce

to the micro-macro moduli relations reported in Diana (2023), Diana et al. (2022) for equivalent Cauchy materials. As previously announced, because of the symmetric nature of strain in standard continua, the relation $C_{1122} = C_{1221}$ is evaded in this case[9] (Diana et al., 2022), as Eq. (56) reduce to those obtained by Diana (2023)

$$C_{1111} = C(19\mathcal{K}_{1111} + 3\mathcal{K}_{2222} + 12\mathcal{K}_{1212} + 2\mathcal{K}_{1122}) \tag{70}$$

$$C_{2222} = C(3\mathcal{K}_{1111} + 19\mathcal{K}_{2222} + 12\mathcal{K}_{1212} + 2\mathcal{K}_{1122}) \tag{71}$$

$$C_{1122} = C(\mathcal{K}_{1111} + \mathcal{K}_{2222} + 4\mathcal{K}_{1212} + 6\mathcal{K}_{1122}) \tag{72}$$

$$C_{1212} = C(3\mathcal{K}_{1111} + 3\mathcal{K}_{2222} + 12\mathcal{K}_{1212} + 2\mathcal{K}_{1122}) \tag{73}$$

$$C_{1112} = 4C(3\mathcal{K}_{1112} + \mathcal{K}_{2212}) \tag{74}$$

$$C_{2212} = 4C(\mathcal{K}_{1112} + 3\mathcal{K}_{2212}) \tag{75}$$

Moreover, it is self-apparent that in the limit case of $C_{1111} = 3C_{1212}$ in isotropic standard elasticity, these relations further reduces to those of the well-known Silling's non-local continuum with central actions (Silling, 2000). Further details can be found in Diana (2023).

It should be mentioned that arbitrary material rotations can be easily taken into account in the proposed model. Consider a micropolar solid, and let $\{\breve{\mathbf{e}}_1, \breve{\mathbf{e}}_2\}$ be an orthonormal basis embedded in the material such that, in the initial configuration, we have $\breve{\mathbf{e}}_1 \equiv \mathbf{e}_1$, $\breve{\mathbf{e}}_2 \equiv \mathbf{e}_2$. For arbitrary rotations of the material, Eqs. (37) and (39) modify substituting the bond angle ψ with the angle difference $\psi - \zeta$, where $\zeta = \mathrm{Arg}\,(\breve{\mathbf{e}}_1 \cdot \mathbf{e}_1 + \imath \breve{\mathbf{e}}_2 \cdot \mathbf{e}_2)$ is positive if denotes a counterclockwise rotation of $\breve{\mathbf{e}}_i$ with respect to $\mathbf{e}_i$. Moreover, in case of achiral orthotropic micropolar media ($\mathbb{D}_2$ or $\mathbb{D}_4$ invariance) with principal material axes in the direction of the unit vectors $\breve{\mathbf{e}}_i$, Eqs. (37) and (38) can be written in the equivalent general reduced form

$$k_n(\psi, \zeta) = \mathcal{K}_{1111}\cos^4(\psi - \zeta) + \mathcal{K}_{2222}\sin^4(\psi - \zeta)$$
$$+ \left(2\mathcal{K}_{1122} + \mathcal{K}_{1212} + 2\mathcal{K}_{1221} + \mathcal{K}_{2121}\right)\sin^2(\psi - \zeta)\cos^2(\psi - \zeta) \tag{76}$$

$$k_t(\psi, \zeta) = \mathcal{K}_{2121}\cos^4(\psi - \zeta) + \mathcal{K}_{1212}\sin^4\psi$$
$$+ \left(\mathcal{K}_{1111} + \mathcal{K}_{2222} - 2\mathcal{K}_{1122} - 2\mathcal{K}_{1221}\right)\sin^2(\psi - \zeta)\cos^2(\psi - \zeta) \tag{77}$$

$$k_b(\psi, \zeta) = \mathcal{K}_{3131}\cos^2(\psi - \zeta) + \mathcal{K}_{3232}\sin^2(\psi - \zeta) \tag{78}$$

---

[9] Under these conditions, Eqs. (50) and (53) implicitly assume that $\hat{\epsilon}_{12} = \hat{\epsilon}_{21}$. Moreover, one obtains $k_a(\psi) = k_b(\psi) = 0$.
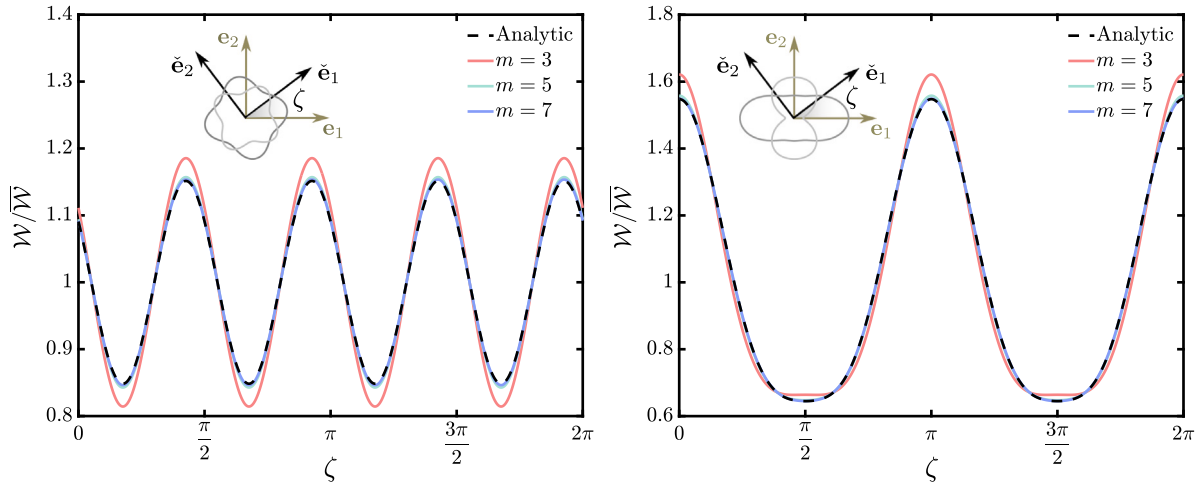
Fig. 3. Normalized macroelastic energy – namely strain energy density – as function of the orientation ζ of the material reference system and corresponding to a simple extension, for increasing values of the density paramenter m. Left: Chiral material with $\mathbb{Z}_4$ invariance; Right: Orthotropic material with $\mathbb{D}_2$ invariance. The micropolar elasticities of the considered homogenized structured materials are reported in Section 3. The gray polar plots refer to the $\zeta = 0$ initial condition.

where the micromoduli given by Eqs. (57)–(62) and Eqs. (67)–(68), are obtained using macro-moduli defined in the material basis $\{\check{\mathbf{e}}_1, \check{\mathbf{e}}_2\}$. Moreover, in case of bi-dimensional *orthotropic chiral* micropolar materials possessing $\mathbb{Z}_4$ or $\mathbb{Z}_2$ invariance (Chen et al., 2014b), the relations (76)–(78) have to be adopted in Eq. (4) together with Eq. (43). It should be noted that in the case of hemitropic solids (Liu et al., 2012) (i.e. micropolar media with SO(2) invariance) these equations, as well as Eqs. (37)–(43) reduce to the directionally-independent scalar functions $k_n = \mathcal{K}_{1111} = \mathcal{K}_{2222}$, $k_t = \mathcal{K}_{2121} = \mathcal{K}_{1212}$, $k_b = \mathcal{K}_{3131} = \mathcal{K}_{3232}$, with the pseudo-scalar $k_a = 2\mathcal{K}_{2221} = 2\mathcal{K}_{1121} = -2\mathcal{K}_{2212} = -2\mathcal{K}_{1112}$ which alternates its sign according to the handedness of the microstructure, while turning out to be vanishing for isotropic micropolar materials (O(2) invariance).

Considering the thermodynamic constraints on the effective material constants in planar micropolar continua (Liu et al., 2012; Chen et al., 2014b), it should be noted that, in general, the micromoduli functions $k_n(\psi)$, $k_t(\psi)$ and $k_b(\psi)$ are required to be non-negative for material and numerical stability (Silling, 2000; Diana, 2023; Diana and Carvelli, 2021). Regarding this point, it should be underlined that Eqs. (37)–(43) derive from a specific assumption, and then other circular functions for detailing the directional dependency of the micromoduli can be adopted, if necessary, provided that conditions imposed by material symmetries are satisfied (Diana, 2023). For instance, the parametric micromoduli functions

$$k_n(\psi, \zeta) = \mathcal{K}_{1111} \cos[(\psi - \zeta)]^{4n} + A\mathcal{K}_{1122} \cos[(\psi - \zeta)]^{2n} \sin[(\psi - \zeta)]^{2n}$$
$$+ \mathcal{K}_{2222} \sin[(\psi - \zeta)]^{4n} \tag{79}$$

$$k_t(\psi, \zeta) = \mathcal{K}_{2121} \cos[(\psi - \zeta)]^{4p} + B\mathcal{K}_{1221} \cos[(\psi - \zeta)]^{2p} \sin[(\psi - \zeta)]^{2p}$$
$$+ \mathcal{K}_{1212} \sin[(\psi - \zeta)]^{4p} \tag{80}$$

$$k_b(\psi, \zeta) = \mathcal{K}_{3232} + (\mathcal{K}_{3131} - \mathcal{K}_{3232}) \cos[(\psi - \zeta)]^{2r} \tag{81}$$

with $A, B \in \mathbb{Z}$, and exponents $n, p, r \in \mathbb{N}^+$ can be suitably particularized to model a wide variety of structured materials homogenized as (orthotropic) micropolar media, while ensuring the requirement above (see also Diana (2023)). Under these conditions, if the rotational invariant part of the elasticity tensor characterizing the orthotropic material results to be not isotropic (e.g. chiral orthotropy with $\mathbb{Z}_2$ and $\mathbb{Z}_4$ invariance (Chen et al., 2014b)), the micropotential term in Eq. (43) is also included in the mathematical expression of the microelastic potential $w(\psi)$. Furthermore, in a similar way to what described above, Eqs. (79)–(80) – in which ζ defines the orientation of the principal material basis of unit vectors $\check{\mathbf{e}}_i$ – assume reduced forms in the limit case of equivalent standard orthotropic continua (with $k_a = k_b(\psi, \zeta) = 0$).

Consider now the discretized system detailed in Appendix. The scalar-valued micromoduli functions have to be evaluated for predetermined values of the virtual fiber angle ψ, such that the direction-dependent pairwise constitutive parameters turn out to be assigned for a finite number of bond directions (Diana, 2023). In the case of regular grids with uniform spacing Δx and given quadrature rule (Seleson, 2014), the number of bond directions to be associated with $k_n(\psi)$, $k_t(\psi)$, $k_b(\psi)$ and $k_a(\psi)$ depends on the density parameter $m = \delta/\Delta x$ (Bobaru, 2011) expressing the ratio between the horizon and the grid spacing considered. It can be noted that larger values of the density parameter require finer angular discretization of the continuous trigonometric functions, which are written in their general form in Eqs. (33)–(36). Therefore, the scalar-valued parameter m should be chosen in such a way that the effective material anisotropy of the micropolar solid under consideration is correctly reproduced by the discretized model (Diana et al., 2022; Diana, 2023). Specifically, given a macro-deformation field defined over the horizon region $H_{\mathbf{x}}$, the macroelastic energy of the discretized CM model should equal the micropolar continuum counterpart (i.e. its elastic energy density) for any arbitrary rigid rotation ζ of the material. As a representative case we consider here a uniaxial extension (affine displacement field over $H_{\mathbf{x}}$ with vanishing uniform micro-rotation) in the direction of the unit vector $\mathbf{e}_1$ of the usual reference basis $\{\mathbf{e}_1, \mathbf{e}_2\}$. The orthogonal basis $\{\check{\mathbf{e}}_1, \check{\mathbf{e}}_2\}$ is considered embedded in the material with the initial condition $\check{\mathbf{e}}_1 \equiv \mathbf{e}_1$ ($\zeta = 0$). A micropolar tetrachiral solid ($\mathbb{Z}_4$ invariance) and a orthotropic achiral solid of $\mathbb{D}_2$ invariance (with $\{\check{\mathbf{e}}_1, \check{\mathbf{e}}_2\}$ being the principal material basis) are considered, whose Cosserat constitutive relations will be shown in detail in Section 3. As Fig. 3 shows, $m > 3$ should be adopted in discretized CM models with overall anisotropic properties to correctly represent the variation of the elastic energy density as function of the material rotation ζ (Diana, 2023). However, it is self apparent that larger values of the density parameter lead to progressively increasing computational costs, since larger turns out to be the corresponding number of non-zero elements in the elastic stiffness operator as well (e.g. Eq. (A.15)) (Ballarini et al., 2018). In what follows, unless otherwise specified, $m = 5$ is adopted, which represents a good compromise between computational cost and accuracy of the elastic problem solution (Diana et al., 2022) (see Fig. 3).

At this point, it should be also noted that the analytical identification of the material micromoduli (namely the micro-macro correspondence scheme) developed in this section is derived by tacitly assuming an unbounded domain, or implicitly referring to material points located in the bulk (Silling, 2000). Actually, material points $\mathbf{x} \in \Omega$ with distance $\check{\mathscr{L}} < \delta$ from the nearest point on the boundary do not have a full
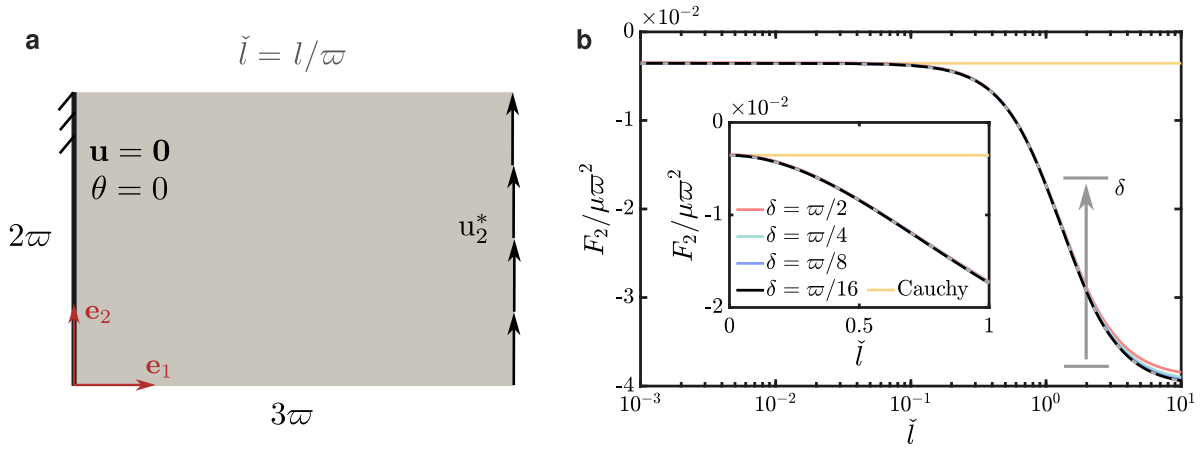
Fig. 4. Thick beam problem in isotropic micropolar elasticity: Layout of the problem and boundary conditions (**a**); Global vertical reaction force F_2 to the imposed displacements of magnitude u_2^* as function of the non-dimensional length-scale parameter $\check{l} = \ell/\varpi$ and corresponding to different horizon size δ (**b**). The micropolar (Cosserat) continuum solution is also reported for reference and denoted by dashed gray line.

horizon region H_x (Silling, 2000), thus their material properties result to be slightly different from those characterizing generic points in the bulk. In order to take into account this important aspect in numerical simulations, a specific surface correction algorithm is required. In this work we refer for simplicity to the volume method by Le and Bobaru (2017), as particularized to our case (Diana, 2023).

3. Benchmark problems

The proposed formulation is validated through several benchmark examples involving homogeneous and non-homogeneous deformation in chiral and achiral micropolar continua with different invariance properties. The nomenclature used for discretized systems as well as the details about the implementation of the CM governing equations based on meshfree approach are detailed in Appendix. The first problem focuses on the analysis of the size-dependent behavior of the continuum-molecular model as referred to the representative case of an isotropic – i.e. O(2) invariance – micropolar (Cosserat) solid under plane strain. In this case, the elastic matrices **C** and **E** can be written in the form

$$\mathbf{C} = \begin{bmatrix} C_{1111} & C_{1122} & 0 & 0 \\ C_{1122} & C_{1111} & 0 & 0 \\ 0 & 0 & C_{1111} - C_{1122} - C_{1221} & C_{1221} \\ 0 & 0 & C_{1221} & C_{1111} - C_{1122} - C_{1221} \end{bmatrix}$$
(82)

$$\mathbf{E} = \begin{bmatrix} E_{3131} & 0 \\ 0 & E_{3131} \end{bmatrix} = \begin{bmatrix} S & 0 \\ 0 & S \end{bmatrix}$$
(83)

with $C_{1111} = C_{2222} = \lambda + 2\mu$, $C_{1122} = \lambda$, $C_{1212} = C_{2121} = C_{1111} - C_{1122} - C_{2121} = \mu + \kappa$ and $C_{1221} = \mu - \kappa$, λ and μ being the Lamé constants, whereas κ and S are the additional micropolar elastic moduli. The elastic modulus relating couple-stress to microcurvatures can be put in the form $S = 4\mu l^2$ (Nakamura and Lakes, 1995) which turns out to be a quadratic function of the characteristic length in bending l, defined as a dimensional parameter related to the size of the heterogeneity of the material homogenized as micropolar medium. In the case of microstructured periodic lattice-like materials, the characteristic length has been shown to be strictly related to the lattice spacing ℓ (Liu et al., 2012; Diana et al., 2023; Kumar and McDowell, 2004). We study the problem of a thick beam (length $L = 3\varpi$ and height $Z = 2\varpi$) with fixed left edge and subjected to an imposed vertical displacement $u^* = L \times 10^{-2}$ along the right edge, as shown in Fig. 5. In order to maximize the resulting overall micropolar effects for same $\check{l}$, $\kappa = \mu$ is assumed for the isotropic material (Wu and Gao, 2023), which is also

characterized by vanishing Poisson's ratio ($\lambda = 0$). The CM solution is compared with the micropolar (Cosserat) continuum solution obtained by finite element (FE) analysis and considering different values of the non-dimensional parameter $\check{l} = l/\varpi$. To this purpose, a FE code is written for the in-plane micropolar elasticity problem, employing eight-node isoparametric quadrilateral elements (Zhang et al., 2005).

It is observed that for relatively small values of the non-dimensional parameter $\check{l}$, the problem turns out to be bending-dominated with resulting overall stiffness and deformed configuration asymptotically convergent to the classical (Cauchy) elasticity solution (Figs. 4–6). Micropolar effects become significant for $\check{l} > 10^{-1}$, such that a substantial increase in flexural stiffness is observed which leads to the progressive increase of the overall stiffness of the body (Fig. 4). Under these conditions (e.g. l is on the order of ϖ), micro-rotation decreases with the decrease of the characteristic length parameter $\check{l}$, while deformation resulting from the imposed displacement goes from being bending-dominated to being shear-dominated. The transition between these different elastic behaviors, which is consistent with results detailed in Wu and Gao (2023), Obrezkov et al. (2022), is clearly visible in Figs. 5–6. When $\check{l} \approx 10$, which is of interest only from a theoretical perspective, the flexural stiffness has increased to the level where bending is almost suppressed insofar the global stiffness is invariant to further increases of the characteristic length parameter $\check{l}$ (Fig. 4) (Deng and Dargush, 2021).

The proposed CM model demonstrates very good accuracy in reproducing the typical size-dependent elastic behavior of planar micropolar elasticity as the computed generalized displacement fields clearly exhibit length-scale sensitivity as well as excellent agreement with Cosserat continuum solution. Moreover, the CM solution shows fast convergence to the micropolar continuum solution as the value of the horizon δ decreases (keeping the density factor m constant). In any case, numerical predictions result to be in accordance with the Cosserat solution even in the case of coarser discretizations, as shown in Fig. 4. Indeed, the CM formulation presented here, together with the micro-macro-correspondence relations detailed in Section 2.1, constitutes a sort of integral-type generalization (accounting for distance actions) of the Cosserat micropolar continuum (Forest, 2005). This (expected) result is consistent with those obtained by continumm-molecular models for standard elasticity (Diana, 2023; Silling, 2000), for which convergence properties to classical (Cauchy) continuum mechanics (for reducing values of the horizon) has been extensively demonstrated (see for instance (Silling, 2000; Silling and Lehoucq, 2008; Bobaru et al., 2009; Diana, 2023)). It is worth noting that while in the CM model for standard media (Diana, 2023), the rotation field $\theta(\mathbf{x})$ reproduces the macro-rotation of classical elasticity (in the limit of δ going to zero),
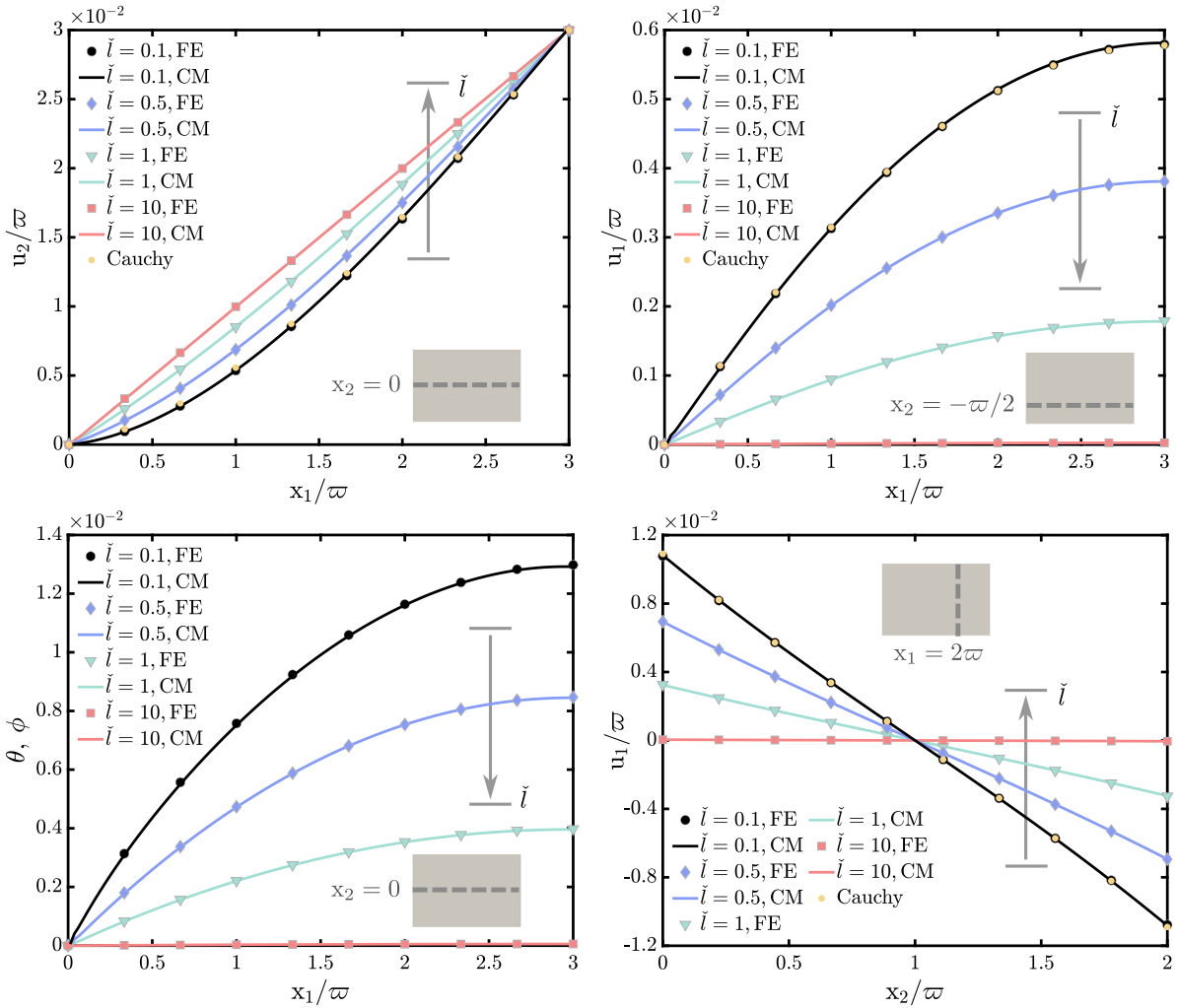
Fig. 5. Thick beam problem in isotropic micropolar elasticity: Non-dimensional vertical displacement u_2/ϖ and rotation θ along the abscissa $x_2 = -\varpi/2$ obtained by the CM model with $\delta = \varpi/8$ for different values of the non-dimensional length-scale parameters $\check{l} = \ell/\varpi$ (first column); Non-dimensional horizontal displacement u_1/ϖ along the abscissae $x_2 = -\varpi/2$ and $x_1 = 2\varpi$ obtained by the CM model with $\delta = \varpi/8$ for different values of the non-dimensional length-scale parameters $\check{l} = l/\varpi$ (second column). The CM solution is compared with the corresponding Cosserat FE solution and Cauchy reference solution with ϕ being the micropolar continuum micro-rotation. CM solution obtained adopting $\delta = \varpi/8$.

here $\theta(\mathbf{x})$ turns out to represent the micro-rotation field of micropolar (Cosserat) elasticity (see Fig. 5).

In order to demonstrate the ability of the proposed CM framework to model size-dependent anisotropic elastic behavior, we consider now the case of a microstructured material homogenized as an orthotropic micropolar continuum. In particular, we refer to a two-dimensional periodic masonry-like material composed of rigid units of finite dimensions (length b and the height a) and linearly elastic interfaces featuring a running-bond type tessellation, with $r = b/a$ being the non-dimensional ratio defining the *shape* of the brick units (Bacigalupo et al., 2021). The elastic parameters of the interfaces are $K_n = k_n \check{d}$, $K_t = k_t \check{d}$, $K_\phi = k_n \check{d}^3/12$, which define their axial, shear and rotational equivalent stiffness, respectively. The normal and tangential stiffness per unit length ($\check{d} = a$ or $\check{d} = b/2$ depending on the coordination direction) of the interfaces are instead denoted by k_n and k_t, respectively. The non-dimensional stiffness ratio of the interfaces is $\alpha = K_t/K_n$. It is worth mentioning that microstructures of this kind also characterize bio-inspired nacre-like composites (Greco et al., 2020; Bertoldi et al., 2008). The continualization procedure detailed in Bacigalupo and Gambarotta (2017), Diana et al. (2023) allows obtaining the governing equations in elastostatics of an equivalent micropolar continuum of $\mathbb{D}_2$ invariance, whose constitutive elastic matrix $\mathbf{C}$ and non-local elastic matrix $\mathbf{E}$ in

the (principal) reference basis $\{\check{\mathbf{e}}_1 = \mathbf{e}_1, \check{\mathbf{e}}_2 = \mathbf{e}_2\}$ read

$$\mathbf{C} = \begin{bmatrix} C_{1111} & C_{1122} & 0 & 0 \\ C_{1122} & C_{2222} & 0 & 0 \\ 0 & 0 & C_{1212} & C_{1221} \\ 0 & 0 & C_{1221} & C_{2121} \end{bmatrix} \tag{84}$$

$$\mathbf{E} = \begin{bmatrix} E_{3131} & 0 \\ 0 & E_{3232} \end{bmatrix} \tag{85}$$

where the non-vanishing moduli are expressed by the analytical relations

$$C_{1111} = \frac{1}{4} r k_n a (4 + \alpha r), \qquad C_{2222} = a k_n \tag{86}$$

$$C_{1212} = \alpha a k_n, \qquad C_{2121} = \frac{1}{4} r k_n a (4\alpha + r) \tag{87}$$

$$E_{3131} = \frac{1}{96} r k_n a^3 \left(5r^3 + 18\alpha r + 8\right), \qquad E_{3232} = \frac{1}{24} k_n a^3 \left(r^2 + 8\alpha r + 2\alpha\right) \tag{88}$$

depending on the constitutive parameters of the interface (α and k_n), on the block shape parameter r and the block dimension a (Diana et al., 2024). Different realistic values of the shape parameter $r = 2$ and $r = 3$ are adopted in this study, with non-dimensional ratio $\alpha = 2/5$ corresponding to an interface made of homogeneous linearly elastic material
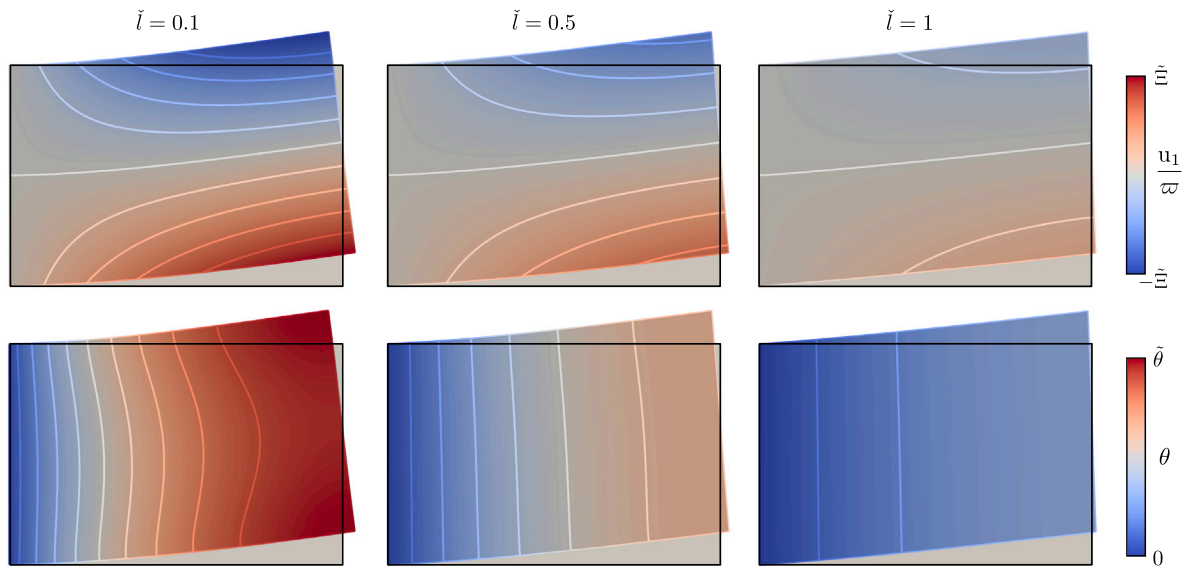
Fig. 6. Thick beam problem is isotropic micropolar elasticity: CM solutions corresponding to non-dimensional length scale parameters $\check{l} = 0.1$, $\check{l} = 0.5$ and $\check{l} = 1$, while adopting $\delta = \varpi/8$. First row: Deformed configuration and horizontal displacement map (with $\tilde{\Xi} = 1.2 \times 10^{-2}$); Second row: Deformed configuration and rotation displacement map (with $\tilde{\theta} = 1.3 \times 10^{-2}$). Contour lines define ten equally-spaced intervals of the variables' range, whereas displacements are magnified by a factor of ten.
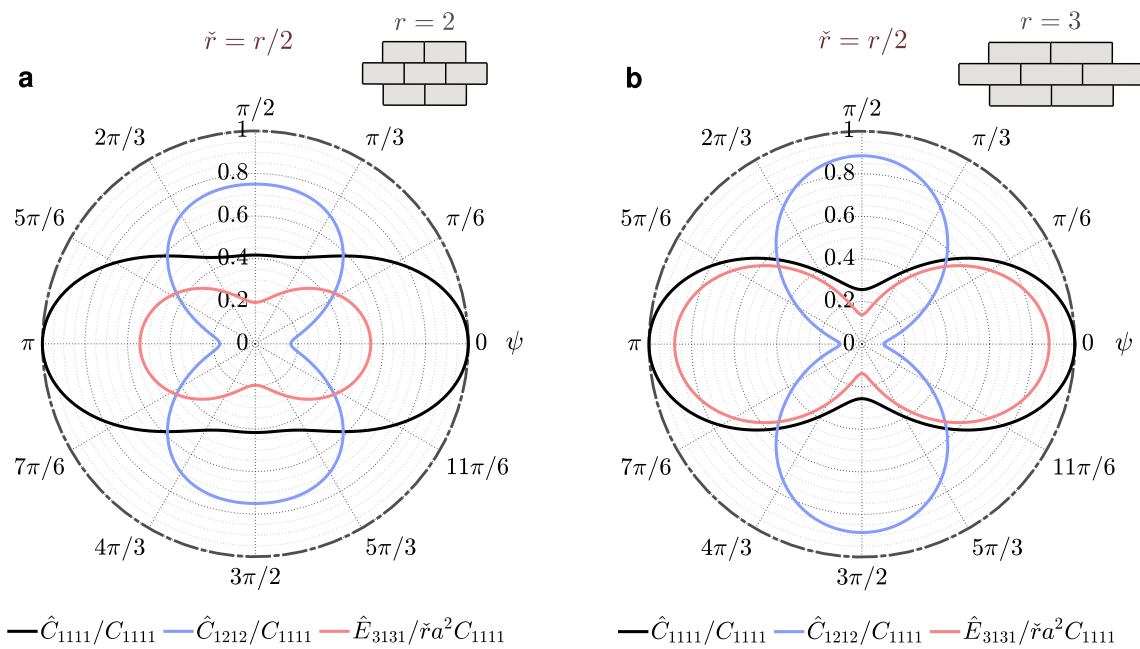
Fig. 7. Shear strip problem in block-lattice masonry-like materials homogenized as orthotropic micropolar solids with $\mathbb{D}_2$ invariance: Polar plots of the off-axis micropolar elastic moduli $\hat{C}_{1111}$, $\hat{C}_{1212}$ and $\hat{E}_{3131}$ in the case of $\alpha = 2/5$ and shape parameter of the blocks $r = 2$ (**a**) and $r = 3$ (**b**).
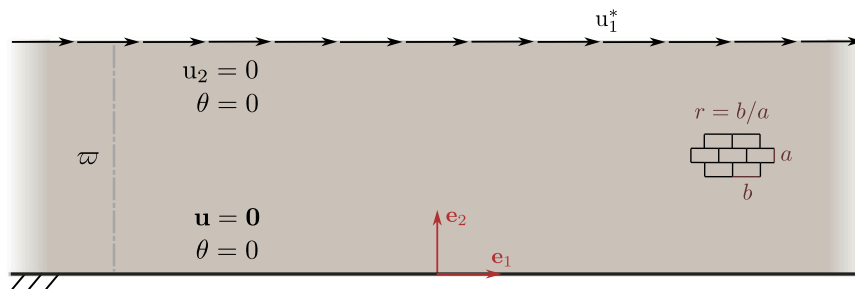
Fig. 8. Shear strip problem in block-lattice masonry-like materials homogenized as orthotropic micropolar solids with $\mathbb{D}_2$ invariance: Layout of the problem and definition of the underlying microstructure considered.
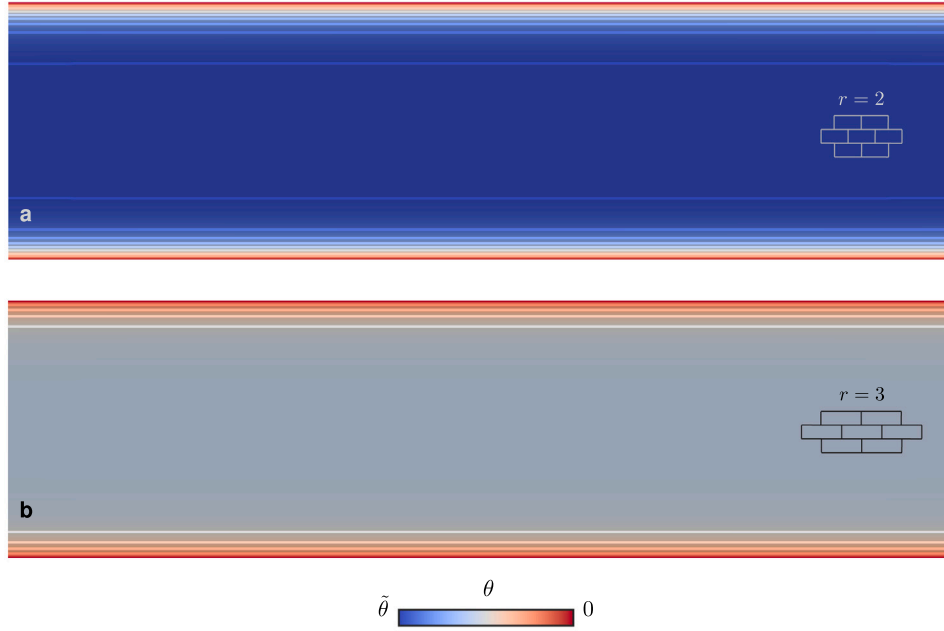
Fig. 9. Shear strip problem in block-lattice masonry-like materials homogenized as orthotropic micropolar solids with $\mathbb{D}_2$ invariance: CM solution (θ field) obtained considering $\alpha = 2/5$ and $\varpi = 10a$ with *shape* parameter $r = 2$ (**a**) and $r = 3$ (**b**). Contour lines define ten equally-spaced intervals of the variables' range, while $\tilde{\theta} = -1.85 \times 10^{-2}$.
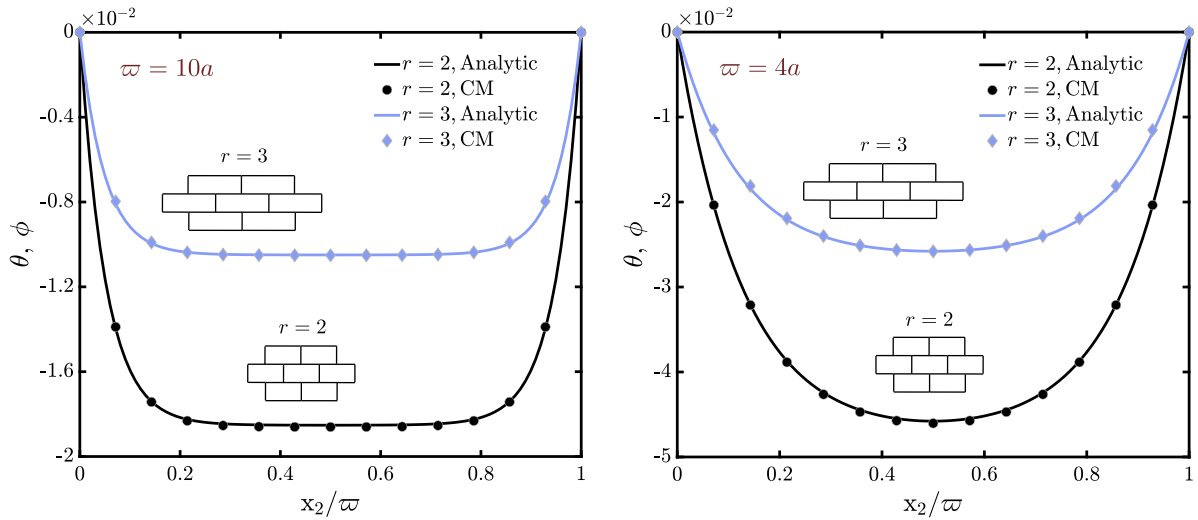
Fig. 10. Shear strip problem in block-lattice masonry-like materials homogenized as orthotropic micropolar solids with $\mathbb{D}_2$ invariance: Analytical and CM solution considering $\alpha = 2/5$, shape parameter $r = 2$ and $r = 3$, α with $\varpi = 10a$ (Left) and $\varpi = 4a$ (Right).

with Poisson's ratio $\nu = 1/5$. Polar plots of the off-axis moduli obtained by Eq. (88) for the two microstructures considered are reported in Fig. 7. Hence, a constrained two-dimensional strip of masonry-like material homogenized as a micropolar continuum, having finite height ϖ and theoretically *unlimited* in the horizontal direction, is considered (Fig. 8) (Bacigalupo and Gambarotta, 2010). The bottom edge is fully restrained, whereas a unitary quasi-static horizontal displacement u_1^* is applied to the top edge (the other degrees of freedom being restrained). Due to the characteristics of the problem and the considered boundary conditions, the generalized displacements turn out to be independent of the horizontal abscissa x_1, whereas the vertical displacements are vanishing. The analytical solution of the micropolar elastic problem in terms of horizontal displacement $u_1(x_2)$ and micro-rotation field $\phi(x_2)$ can be expressed as

$$u_1\left(x_2\right) = c_1 + c_2 x_2 + c_3 e^{\frac{b}{a} x_2} + c_4 e^{-\frac{b}{a} x_2} \tag{89}$$

$$\phi\left(x_2\right) = -\frac{1}{a\left(b^2 + \alpha\right)} c_2 \alpha a + c_3 b\left(\alpha + b^2\right) e^{\frac{b}{a} x_2} + -c_4 b\left(\alpha + b^2\right) e^{-\frac{b}{a} x_2} \tag{90}$$

where a and b are auxiliary variables such that

$$a^2 = \frac{1}{24}\left(r^2 + 8\alpha r + 2\alpha\right), \quad b^2 = \frac{1}{4} r(4\alpha + r), \tag{91}$$

whereas c_1, c_2, c_3, c_4 are constants that can be determined from the four boundary condition equations $u_1(0) = 0$, $u_1(\varpi) = 0$, $\phi(0) = 0$ and $\phi(\varpi) = 0$ (Bacigalupo et al., 2021).

The constrained strip domain is discretized using a CM regular grid with $\delta = \varpi/8$ (see previous benchmark problem), and considering a lateral length $L = 10\varpi$ in such a way to avoid perceptible boundary effects at $x_1 = 0$. We compare the analytical solution in terms of micro-rotation $\phi(x_2)$ of the homogenized microstructured materials, which is characterized by rapid transition of values along the height ϖ, with the $\theta(x_2)$ field obtained by the discretized CM model. In this case, the
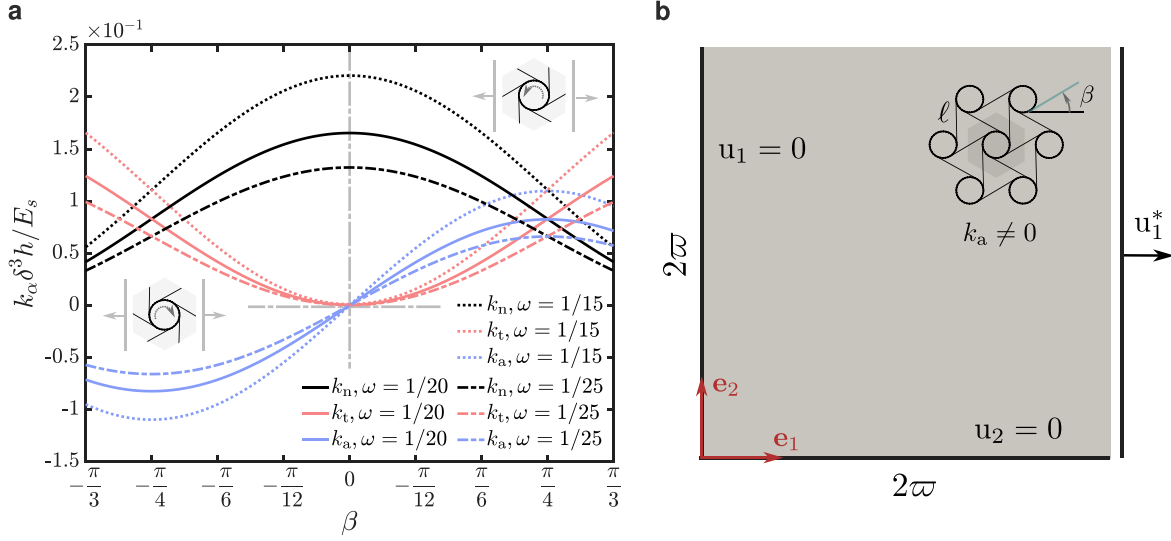
Fig. 11. Hexagonal chiral honeycombs homogenized as micropolar planar chiral solids with SO(2) invariance (Liu et al., 2012); CM micromoduli (see Section 2.1.1) as function of the chirality angle β of the corresponding discrete lattice, and in the case of three different values of the slenderness ratio of the lattice ligaments ω (**a**); Layout of the elastic problem considered (imposed displacement $u_1^* = \varpi/5$) involving affine displacement field with vanishing microcurvature (**b**).

parametric generalized micromodulus functions given by Eqs. (79)–(81) are adopted to describe the overall anisotropy of the material while ensuring the thermodynamically-consistency of the microelastic constitutive relations (Diana, 2023) (see Section 2.1.1). In particular, $A = 1$, $B = 0$ with $n = 2$, $p = 1$, $r = 1$ and $n = 3$, $p = 2$, $r = 3$ are adopted in the case of shape parameter $r = 2$ and $r = 3$, respectively. In order to underline the influence of the microstructure properties as well as the length-scale sensitivity of the micropolar elastic solution, two different strip heights are considered ($\varpi = 4a$ and $\varpi = 10a$) together with the two aforementioned values of the shape parameters r. It is noted that the size of the problem influences the smoothness of the solutions, thus the decay of the micro-rotation from the horizontal boundaries to the center of the constrained strip. On the contrary, the slenderness of the blocks has primary influence on the average magnitude of the resulting micro-rotation field along the height of the strip (Figs. 9–10). Results obtained by the CM formulation are in very good agreement with the analytical solutions corresponding to the representative cases of materials considered. Hence, the CM model for micropolar planar elasticity shows high accuracy in reproducing the size-dependent behavior of microstructured materials homogenized as micropolar continua accounting for their directional dependent elastic properties, as shown in Figs. 9–10.

Consider now the case of a hemitropic bi-dimensional material. In particular, we refer here to the well-known hexagonal chiral honeycombs (Prall and Lakes, 1997) consisting of periodic patterns of (rigid) circles linked by straight elastic beam-like ligaments homogenized as micropolar continua with SO(2) invariance (Liu et al., 2012; Chen et al., 2014b; Bacigalupo and Gambarotta, 2014). The resulting effective constitutive tensor **E** takes the same form as Eq. (83), whereas the general form of **C** in this case reads

$$\mathbf{C} = \begin{bmatrix} C_{1111} & C_{1122} & C_{1112} & -C_{1112} \\ C_{1122} & C_{1111} & C_{1112} & -C_{1112} \\ C_{1112} & C_{1112} & C_{1111} - C_{1122} - C_{1221} & C_{1221} \\ -C_{1112} & -C_{1112} & C_{1221} & C_{1111} - C_{1122} - C_{1221} \end{bmatrix} \tag{92}$$

which turns out to be invariant under arbitrary rotations of the reference basis, but not to mirror reflections (see Section 2.1). In this case, mirror reflection operations lead to sign inversion of the moduli $C_{1112}, C_{1121}, C_{2212}$ and C_{2221}, the elastic matrix **C** being coincident to

its hemitropic part (Zou et al., 2001). In other words, these constants alternate their signs according to the handedness of the microstructure (see Fig. 11).

According to Liu et al. (2012), Bacigalupo and Gambarotta (2014) the elastic matrix **C** may be written, alternatively, as

$$\mathbf{C} = \begin{bmatrix} 2\mu + \lambda & \lambda & -A & A \\ \lambda & 2\mu + \lambda & -A & A \\ -A & -A & \mu + \kappa & \mu - \kappa \\ A & A & \mu - \kappa & \mu + \kappa \end{bmatrix} \tag{93}$$

where the following moduli are analytically defined

$$\mu = \frac{\sqrt{3}}{4} \breve{a} E_s \omega \left(1 + \omega^2\right) \qquad \lambda = \frac{\sqrt{3}}{4} \breve{a} E_s \omega \left(1 - \omega^2\right) \cos 2\beta \tag{94}$$

$$\kappa = \frac{\sqrt{3}}{2} \breve{a} E_s \omega \left[\sin^2 \beta + \omega^2 \cos^2 \beta\right] \qquad A = \frac{\sqrt{3}}{4} \breve{a} E_s \omega \left(1 - \omega^2\right) \sin 2\beta \tag{95}$$

with β being the chirality angle (e.g. the smallest angle between the line connecting the centroids of two neighboring rigid circles and the corresponding ligament of lenth ℓ), $\omega = o/\ell$ the non-dimensional (slenderness) ratio between the ligament in-plane thickness o and the length ℓ, and $E_s = E_b/\left(1 - \nu_b^2\right)$ or $E_s = E_b$ under plane strain or plane stress assumptions, respectively (E_b and ν_b are the Young's modulus and Poisson's ratio of the lattice) (Liu et al., 2012; Bacigalupo et al., 2023). The non-dimensional parameter $\breve{a}$ denotes the ratio between the out-of plane thickness of the ligaments to that of the rigid circles of diameter $\breve{D} = \ell \tan \beta$ (Bacigalupo et al., 2023). The constitutive matrix **C**, as written in Eq. (93), is that of a hemitropic planar solid characterized by *positive* chirality when $\beta > 0$ (i.e. tensile bulk strain leads to positive-defined counterclockwise micro-rotation with $A > 0$). In our case, $E_{3131} = S = \sqrt{3}\breve{a} E_s \omega \ell^2 (4\omega^2 + 3 \tan^2 \beta)/12$. We consider hexagonal chiral lattices characterized by three realistic values of the slenderness ratio ω while assuming chirality angles ranging from $\beta = -\pi/3$ to $\beta = \pi/3$, with $\breve{a}$ being unitary. The CM micromoduli are determined using Eq. (93) and the analytical micro-macro correspondence procedure detailed in Section 2.1.1 particularized to the case of hemitropic solids. Actually, in this case the directional invariant micromodulus k_a in Eq. (43) turns out to be non vanishing, as the pseudo-scalar defined in Section 2.1 is $C_{\mathscr{H}} = 2A$. As shown in Fig. 11, the resulting directional independent micromoduli k_n and k_t are even function of the chirality angle β (see Fig. 12) characterizing the underlying microstructure. Conversely, the micromodulus k_a turns out to be a odd function of β, and it reverses
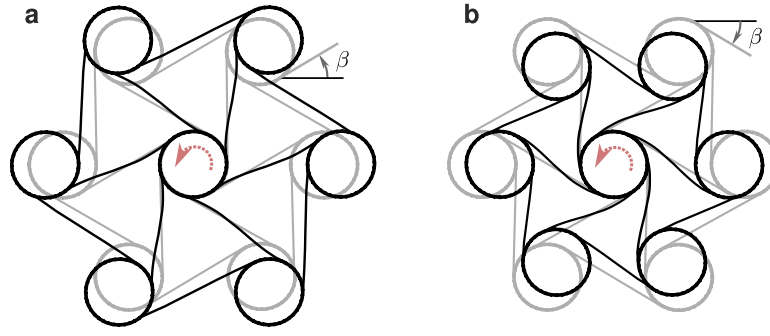
Fig. 12. Hexagonal chiral honeycombs made of rigid rings and slender beam-like elastic ligaments: Elastic coupling between (ring) rotation and equivalent overall bulk strain in the case of *positive* ($\beta > 0$) chirality (**a**) and *negative* ($\beta < 0$) chirality (**b**).
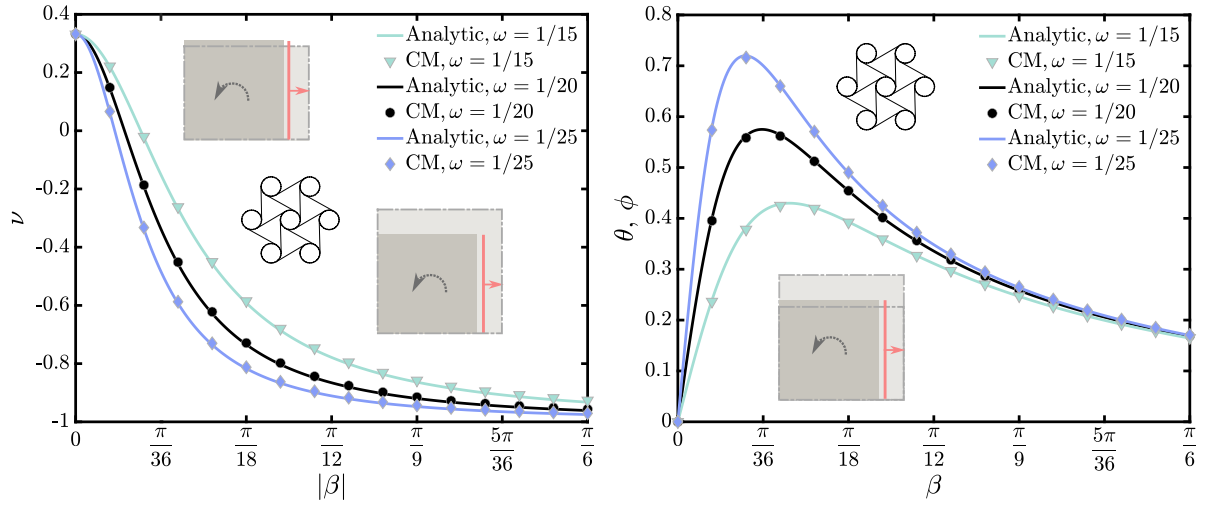

Fig. 13. Hexagonal chiral honeycombs homogenized as micropolar planar chiral solids with SO(2) invariance (Liu et al., 2012) under uniaxial extension; Analytic and CM values of the resulting Poisson's ratio of the chiral micropolar solid as function of the chirality angle β (Left); Analytic micro-rotation ϕ and CM rotation θ as function of β (Right). Only positive values of the chirality angle are considered here as the Poisson's ratio turns out to be an even function of β whereas the micro-rotation results to be a odd function of the same angle.

its sign when the microstructure is reversed as well (Fig. 11). It can be noted that, as a result of the conceived micro-macro correspondence scheme, k_n, k_t and k_a exhibit similar analytical dependency on β as the macro-constants C_{1111}, C_{1212} and $C_{\mathcal{H}}$, respectively. The Layout of the elastic problem considered is reported in Fig. 11. The imposed boundary conditions lead to theoretical affine displacements and vanishing microcurvature field. In this case, the exact solution of the elastostatic problem in terms of (uniform) micro-rotation $\phi(\mathbf{x}) = \phi$ reads

$$\phi = \frac{(1-\nu)A\varepsilon_{11}^*}{2\kappa} = \frac{(1-\nu)Au^*}{2\kappa\varpi} = \frac{(1-\omega^4)\sin(2\beta)u^*}{[2(\omega^4-1)\cos(\beta)^2 + 2(3\omega^2+1)]\varpi} \quad (96)$$

with ν being the overall Poisson's ratio (plane stress conditions are assumed) defined as

$$\nu = \frac{A^2 - \kappa\lambda}{A^2 - (2\mu + \lambda)\kappa} \quad (97)$$

The micro-rotation and the resulting overall Poisson's ratio derived from Eqs. (96)–(97) and characterizing the chiral micropolar continuum (i.e. the homogenized microstructured chiral lattice) are compared with the corresponding values computed by the proposed CM model. In this case, the overall Poisson's ratio is obtained as $\nu = -\tilde{u}_2/\tilde{u}_1$, with $\tilde{u}_1$ and $\tilde{u}_1$ being the displacement components at $x_1 = x_2 = \varpi$. Results shown in Figs. 13 demonstrate that the CM model is capable to reproduce with accuracy the coupling behavior between bulk strain and micro-rotation typical of micropolar chiral planar solids, and uncovered by classical elasticity (see Fig. 12). Moreover, the micropotential term $w_{s\gamma}$ introduced in Section 2 is able to describe the resulting strong

auxeticity of the material as well (Fig. 13). It is worth to underline that the aforementioned overall elastic behaviors arise naturally as a result of properly-defined constitutive relations produced for micro interactions (i.e the virtual fibers). In other words, as opposed to the phenomenological approach of continuum mechanics, the CM approach leads to a mechanism-based description of auxeticity and chirality. As last validation example, we consider the case of an anisotropic two-dimensional chiral solid. We refer to the tetrachiral block-lattice material (Bacigalupo and Gambarotta, 2020; Diana et al., 2023) already mentioned in Section 2.1.1, and made up of periodic tessellations of square rigid units of side a, inclined by the chirality angle $\beta(-\pi/4 < \beta < \pi/4)$, and connected by elastic interfaces of length $b = (1 - \tan\beta)a$ and vanishing thickness (see Fig. 14). Similarly to the previous case, the chirality angle β is defined as the smallest angle between the line connecting the centroids of two neighboring blocks and the line perpendicular to the corresponding elastic interface. The axial, shear and rotational overall stiffness of the interfaces are $K_n = k_n b$, $K_t = k_t b$, $K_\phi = k_n b^3/12$, respectively (Bacigalupo and Gambarotta, 2020). Considering the usual reference basis $\{\mathbf{e}_1, \mathbf{e}_2\}$, the elastic matrices of the equivalent micropolar continuum of $\mathbb{Z}_4$ invariance, as identified analytically by Diana et al. (2023), read

$$\mathbf{C} = \begin{bmatrix} C_{1111} & C_{1122} & C_{1112} & C_{1121} \\ C_{1122} & C_{1111} & -C_{1121} & -C_{1112} \\ C_{1112} & -C_{1121} & C_{1212} & C_{1221} \\ C_{1121} & -C_{1112} & C_{1221} & C_{1212} \end{bmatrix} \quad (98)$$
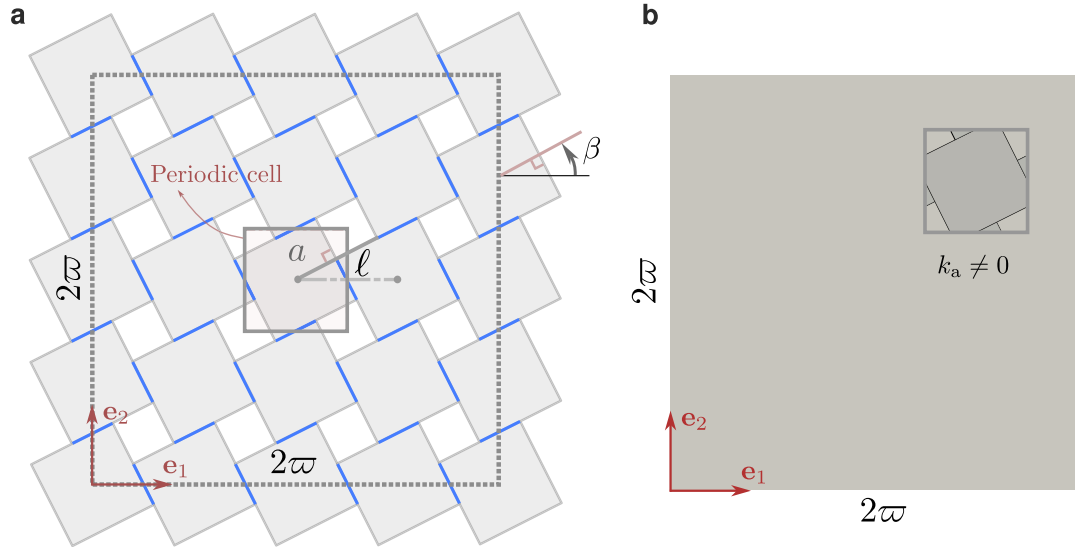
Fig. 14. Tetrachiral periodic block-lattices (Bacigalupo and Gambarotta, 2020) homogenized as micropolar continua with $\mathbb{Z}_4$ invariance: Discrete square tessellation of 5×5 rigid units and elastic interfaces with indication of the periodic cell (**a**). Two-dimensional domain of the equivalent chiral micropolar continuum considered for the elastostatic problems whose boundary conditions are detailed in Table 1 (**b**).

$$\mathbf{E} = \begin{bmatrix} E_{3131} & 0 \\ 0 & E_{3131} \end{bmatrix} \tag{99}$$

the non-vanishing moduli being

$$C_{1111} = \mathsf{K}_n \left(\cos^2 \beta + \alpha \sin^2 \beta \right) \quad C_{1121} = \mathsf{K}_n \left(1 - \alpha \right) \sin \beta \cos \beta \tag{100}$$

$$C_{1212} = \mathsf{K}_n (\sin^2 \beta + \alpha \cos^2 \beta) \quad E_{3131} = \left[\mathsf{K}_\phi + \tilde{\lambda} \ell^2 \mathsf{K}_n \left(\sin^2 \beta + \alpha \cos^2 \beta \right) \right] \tag{101}$$

which depends on the constitutive parameters of the interface K_n and α (e.g. the usual non-dimensional stiffness ratio), on the block centroid distance or lattice-spacing $\ell = a/\cos \beta$, and on the chirality angle β, with $\tilde{\lambda} = 1/12$. In this case, we consider two elastostatic problems defined over the continuum square domain of side 2ϖ reported in Fig. 14, and characterized by different sets of boundary conditions (e.g. $\mathscr{P}_1$ and $\mathscr{P}_2$) detailed in Table 1. The same elastic problems, the displacements being affine and the micro-rotations being uniform, are also solved for the full-discrete Lagrangian model of the periodic mechanical metamaterial (Bacigalupo and Gambarotta, 2020) featuring a square periodic tessellation of rigid units and elastic interfaces (Fig. 14). Since the resulting microcurvature field turns out to be vanishing, the elastostatic problems result to be size-independent and then the choice of the lattice spacing ℓ does not affect the solution. For illustrative purposes, a square tessellation of 5×5 rigid blocks and elastic interfaces is adopted in this case, which corresponds to the lattice spacing $\ell = \varpi/2$. Two different values of the non-dimensional stiffness ratio of the interface are considered (i.e. $\alpha = 1/2$ and $\alpha = 1/4$) while the chirality angle is varied within the range $\beta(-\pi/4 < \beta < \pi/4)$. It is noted that, due to $\mathbb{Z}_4$ invariance of the material, when inverting the chirality angle β, the pseudo-scalar $C_{\mathscr{H}}$ together with the angle ζ defining the principal direction of unit vector $\check{\mathbf{e}}_1$ such that $\max \hat{C}_{1111} = \check{C}_{1111}$, reverse their sign. The latter condition influences the resulting overall anisotropic properties of the material (Fig. 15). The microelastic constants of the CM model are derived using Eqs. (57)–(69) with the corresponding standard direction dependent micromoduli functions given by Eqs. (37)–(43) in the case of $\alpha = 1/2$. Moreover, in order to show the effectiveness of the generalized parametric directional dependent functions for orthotropic materials with chirality, while ensuring positive-definiteness of the microelastic constants as discussed in Section 2.1.1, Eqs. (79)–(81) with $\mathsf{A} = \mathsf{B} = 1$, $n = 4$, $p = 2$, $r = 1$ are adopted in the case of $\alpha = 1/4$. The corresponding microelastic constants are analytically determined using Eqs. (47) and (55), via energy-based procedure as

Table 1
Tetrachiral periodic block-lattices homogenized as micropolar continua with $\mathbb{Z}_4$ invariance: Elastic problem defined by boundary conditions on the four edges of the square domain in Fig. 14 and corresponding to two different cases involving theoretical affine displacements and uniform rotations.

Case/Problem	left ($x_1 = 0$)	right ($x_1 = 2\varpi$)	bottom ($x_2 = 0$)	top ($x_2 = 2\varpi$)
$\mathscr{P}_1$	$\mathbf{u} = \mathbf{0}$	$u_1 = \varpi/5$	free	free
$\mathscr{P}_2$	$u_1 = 0$	$u_1 = \varpi/5$	$u_2 = 0$	$u_2 = \varpi/5$

detailed in Section 2.1.1. In the case of problem $\mathscr{P}_1$, the imposed boundary conditions lead to the affine transversal displacement field analytically given for an equivalent micropolar continuum by

$$u_2(x_1) = \frac{6\tilde{\lambda}(\alpha - 1)\cos \beta \sin \beta}{5(\sin^2 \beta + \alpha \cos^2 \beta)} x_1 \tag{102}$$

while the (uniform) micro-rotation $\phi(\mathbf{x}) = \phi$ turns out to be vanishing, the elastic response being in this case basically governed by material anisotropy. Considering instead the problem $\mathscr{P}_2$, the imposed equivalent uniform expansion leads to the uniform micro-rotation field analytically given by

$$\phi = \frac{6\tilde{\lambda}(1 - \alpha)\cos \beta \sin \beta}{5(\sin^2 \beta + \alpha \cos^2 \beta)} \tag{103}$$

the mechanical response of the lattice-like material being influenced by its chiral properties (owing to SO(2) invariance of $\mathbf{C}_o$ in Eqs. (32)) as the characteristic direct elastic coupling between bulk strain and pure rotation appears (Chen et al., 2014b) (see Fig. 16). The numerical solutions obtained using the CM model and corresponding to the elastic problems $\mathscr{P}_1$ and $\mathscr{P}_2$ with the aforementioned assumed parameters result to be in excellent agreement with the analytical micropolar continuum solution in Eqs. (102)–(103), as well as with the solution of the governing equations of the discrete Lagrangian tetrachiral block-lattice system (Bacigalupo and Gambarotta, 2020) (Fig. 17).

An additional size-dependent problem, whose layout is detailed in Fig. 18, is also considered for the tetrachiral lattice homogenized as micropolar medium with $\mathbb{Z}_4$ invariance, involving this time inhomogeneous deformation and non-uniform microcurvature field. The size-dependent problem is solved considering two different values of the length scale parameter ℓ characterizing the underlying material microstructure (i.e. $\ell = \varpi/2$ and $\ell = \varpi/10$), and directly associated with the block-lattice dimensions. The assumed reference values of
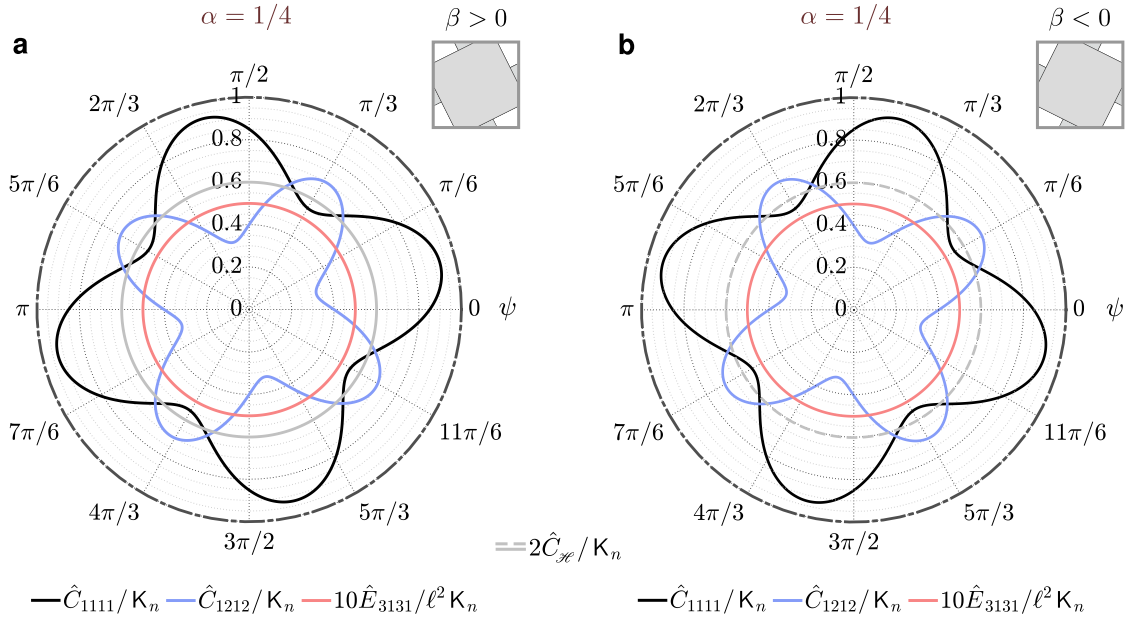
Fig. 15. Tetrachiral periodic block-lattices homogenized as micropolar continua with $\mathbb{Z}_4$ invariance: Polar plots of the off-axis micropolar elastic moduli $\hat{C}_{1111}$, $\hat{C}_{1212}$, $\hat{E}_{3131}$ and $\hat{C}_{\mathscr{H}} = C_{\mathscr{H}}$ in the case of $\alpha = 1/4$ and chirality angle $\beta = \arctan(1/2)$ (**a**) and $\beta = -\arctan(1/2)$ (**b**). Dashed lines indicate negative values.
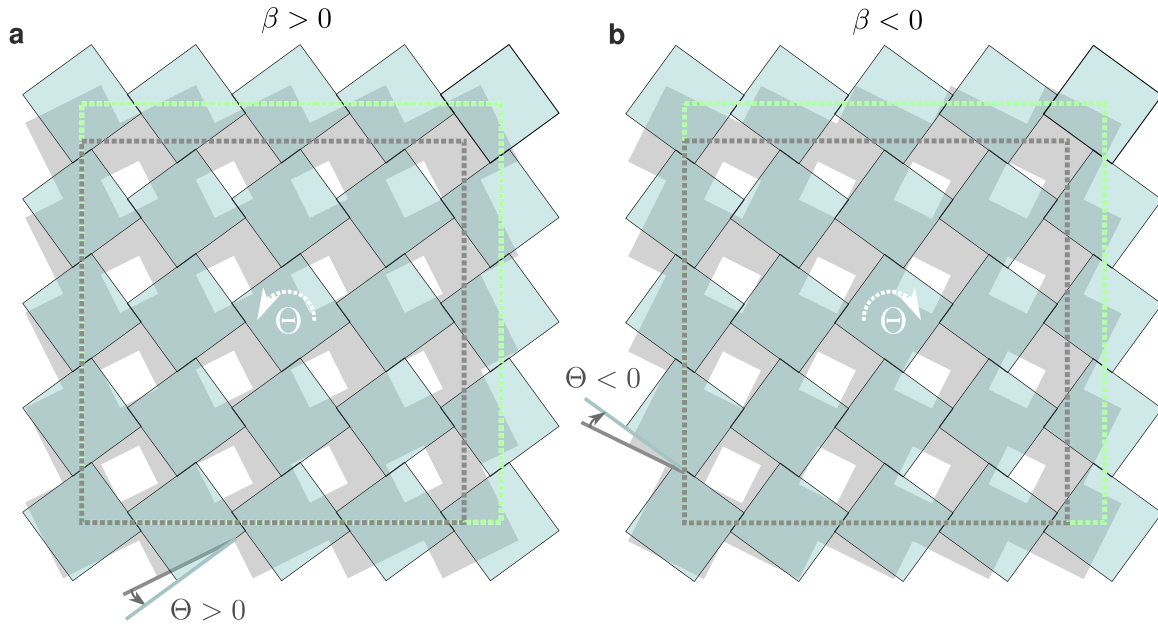

Fig. 16. Tetrachiral block-lattice ($\mathbb{Z}_4$ invariance) with $\alpha = 1/4$ and chirality angle $\beta = \pm\arctan(1/2)$ subjected to equivalent uniform expansion (problem $\mathscr{P}_2$): The bulk deformation leads to uniform counterclockwise blocks rotations in case of $\beta > 0$ (**a**), and uniform clockwise blocks rotations in case of $\beta < 0$ (**b**). Rotations are magnified by a factor of two for better visualization.

the non-dimensional stiffness and chirality angle are $\alpha = 1/4$ and $\beta = -\arctan(1/2)$, respectively. As shown in Figs. 18–20, the material length-scale parameter ℓ leads to two main important effects in the global material response. Actually, lower values of the internal length accentuate the asymmetry of the resulting elastic response of the material as well as the localization of the deformation in a smaller zone close to the load-application area (see Fig. 20). It is noted that, in the case of $\ell = \varpi/10$, the resulting displacement field turns out to be slightly influenced by micropolar effects sufficiently far from the top boundary (Fig. 19). In any case, models associated with classical Cauchy continuum are in no way capable to reproduce the characteristic microrotation field influenced by chiral-type elastic coupling effects in the microstructured material. Results obtained confirm the effectiveness of

the proposed CM formulation and its ability to describe the mechanical behavior of planar anisotropic chiral micropolar media under general inhomogeneous deformation.

3.1. Crack nucleation and propagation

In this last section we investigate the size effect of elasticity and energy dissipation during the crack nucleation and propagation in two-dimensional micropolar media. The classical single-edge notched tension and shear tests are considered to this purpose, with layout and boundary conditions detailed in Fig. 21. We assume, without loss of generality, an isotropic micropolar solid (O(2) invariance) with $\kappa = \mu = 105$ GPa and $\lambda = 0$ (see Eq. (82) and Section 3), the resulting Young
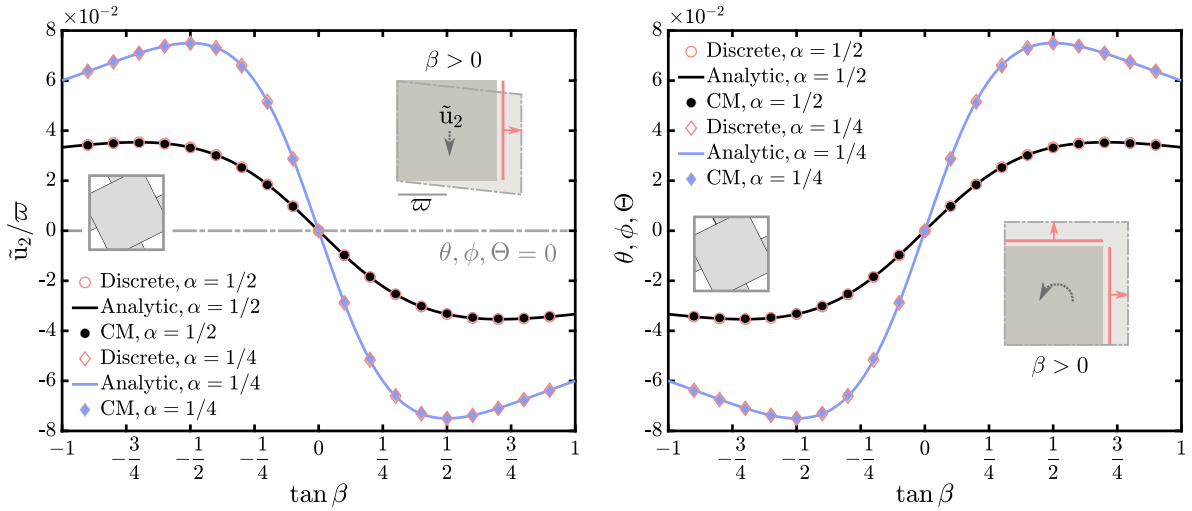
Fig. 17. Tetrachiral periodic block-lattices homogenized as micropolar continua with $\mathbb{Z}_4$ invariance: Vertical displacement $\tilde{u}_2$ obtained by analytical solution, CM and full-discrete models, as function of the chirality angle β and corresponding to the problem/case $\mathcal{P}_1$ in Table 1 (left); Analytic micro-rotation ϕ, CM rotation θ and discrete block rotation Θ as function of the chirality angle β and corresponding to the problem/case $\mathcal{P}_2$ in Table 1 (right).
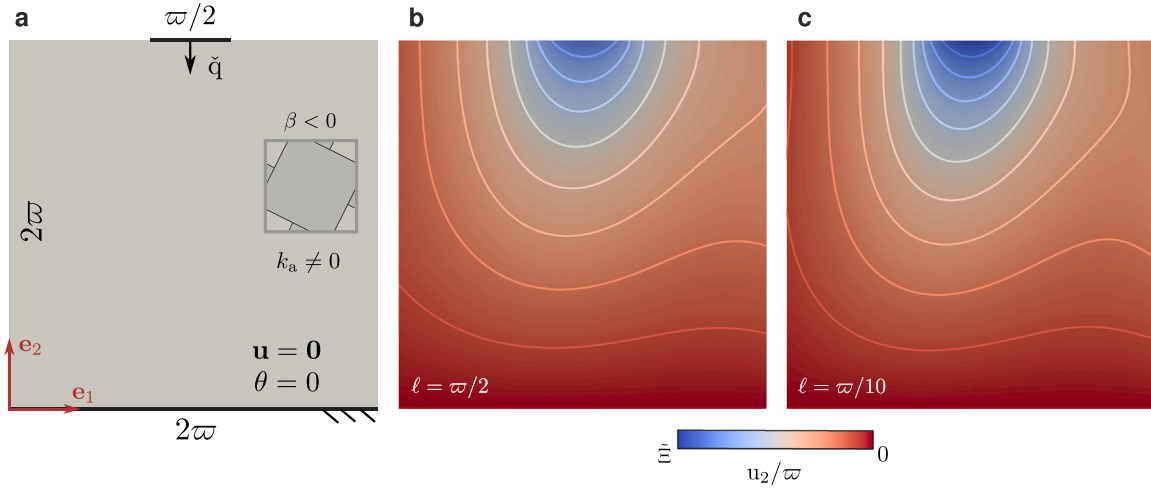
Fig. 18. Tetrachiral periodic block-lattices ($\mathbb{Z}_4$ invariance): Layout of the elastic problem defined for the homogenized micropolar medium and involving inhomogeneous deformation (a); Vertical displacement map obtained by the CM model in the case of structured material with $\ell = \varpi/2$ (b) and $\ell = \varpi/10$ (c); The assumed non-dimensional stiffness and the chirality angle are $\alpha = 1/4$ and $\beta = -\arctan(1/2)$, respectively, whereas $\check{q} = K_n h/10$ with $\tilde{\Xi} = -\pi/20$. Contour lines define ten equally-spaced intervals of the variables' range.

modulus and Poisson's ratio being $E = 210$ GPa and $\nu = 0$, respectively. The considered values for the micropolar internal length as defined at the beginning of Section 3 are instead $l = \varpi/50$, $l = \varpi/10$ and $l = \varpi/5$. It can be noted that the here assumed conditions allow the resulting overall micropolar effects for same $\check{l}$ to be maximized (see Section 3), whereas length-scale effects on fracture result to be isolated from those related to the elastic anisotropy of the material.

Focusing on brittle fracture, we provide a mechanism-based description of crack nucleation and propagation in micropolar solids using an energy-based failure criterion (Diana and Ballarini, 2020; Foster et al., 2011) characterized by the definition of a critical scalar-valued function $w_c(\mathbf{x}, \mathbf{x}', \zeta) = w_c(\psi, \zeta)$ of the bond total stored energy density defined in Eq. (4). The energy-based criterion adopted considers the instantaneous bond or virtual fiber failure when the scalar-valued critical micropotential energy function $w(\mathbf{x}, \mathbf{x}', t)$ attains its critical value $w_c(\psi, \zeta)$, which, in general, result to be direction-dependent (Diana, 2023). Assuming for simplicity that the material resistance to fracture is uniform, the angular-independent critical value w_c is derived analytically by equating the fracture energy $\mathcal{G}_c$ to the total work required to break all the bonds per unit fracture area (with fracture *surface* having arbitrary

orientation in the considered special case) (Diana, 2023). Consider the generic plane $\hat{\pi}$ passing through $\hat{\mathbf{x}}$, and z be the distance between $\hat{\pi}$ and the generic point $\mathbf{x}$ along the positive axis perpendicular to $\hat{\pi}$ and passing through $\hat{\mathbf{x}}$ as well (Silling and Askari, 2005; Diana and Ballarini, 2020). Hence, the following relation holds

$$\mathcal{G}_c = \int_0^\delta \int_z^\delta \int_{-\mathcal{I}}^{\mathcal{I}} w_c(\psi, \zeta)\, h\|\xi\|\, d\psi\, d\xi\, dz \qquad (104)$$

where $\mathcal{I} = \arccos z/\|\xi\|$, whereas $w_c(\psi, \zeta) = w_c$ under the assumed hypotheses[10] (for further details about the computation of the integral in Eq. (104) refer to Silling (2000), Diana (2023)). From Eq. (104) one

---

[10] When considering directionally non-uniform fracture resistance, the parametric critical function $w_c(\psi, \zeta) = w_{c2} + (w_{c1} - w_{c2})\cos^n[\mathcal{F}(\psi - \zeta)]$ with $\mathcal{F} \in \mathbb{N}^+$ frequency parameter can be adopted, which allows to model different angular-dependent behaviors (Rezaei et al., 2021; Diana, 2023). In this case, given the orientation of the generic fracture plane π, Eq. (104) should be particularized depending on the specific orientation of the material as defined by the angle ζ (Diana, 2023).
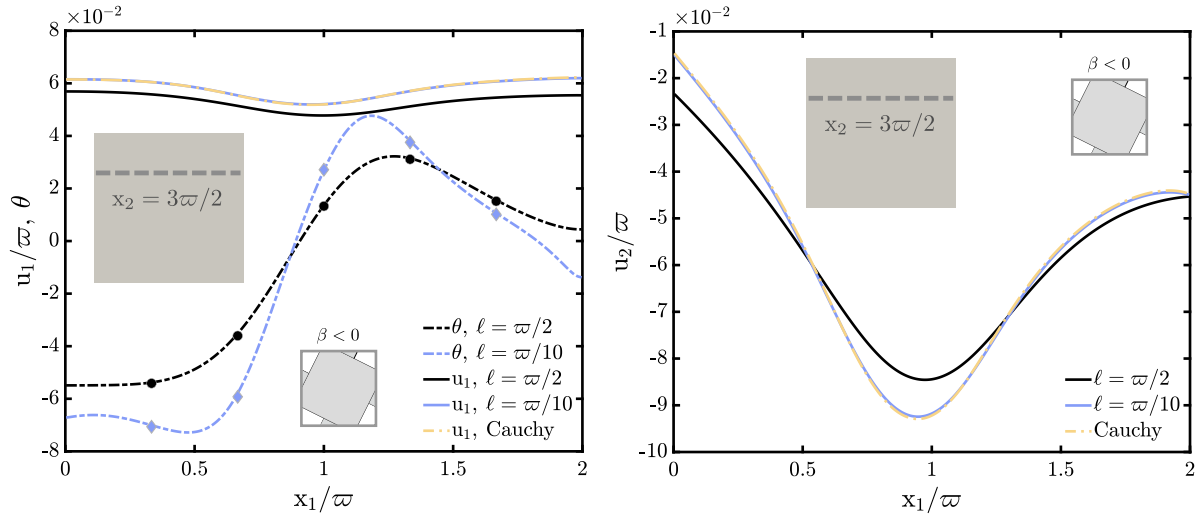
Fig. 19. Tetrachiral periodic block-lattices ($\mathbb{Z}_4$ invariance): Normalized displacements and rotation θ obtained by the CM model along the abscissa $x_2 = 3\varpi/2$ in the case of structured material with non-dimensional stiffness $\alpha = 1/4$ and chirality angle $\beta = -\arctan(1/2)$ under inhomogeneous deformation. The FE micropolar solution in terms of micro-rotation ϕ is also reported for reference and denoted by filled dots ($\ell = \varpi/2$) and filled diamonds ($\ell = \varpi/10$).
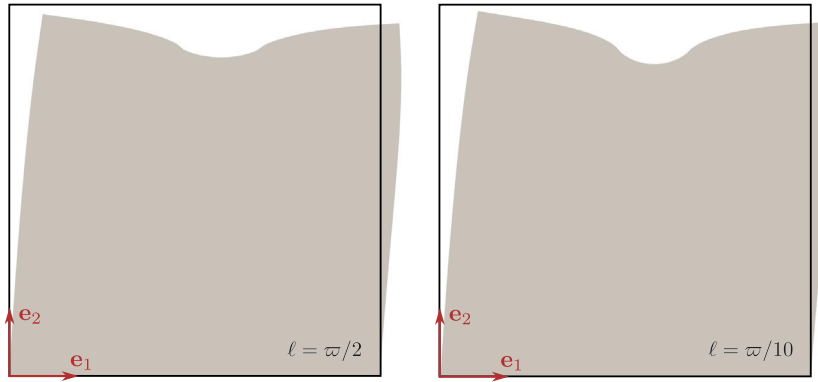
Fig. 20. Tetrachiral block-lattice ($\mathbb{Z}_4$ invariance): Deformed configuration (corresponding to the elastic problem defined for the homogenized micropolar medium and involving homogeneous deformation) obtained by the CM model in the case of $\ell = \varpi/2$ (left) and $\ell = \varpi/10$ (right); The assumed non-dimensional stiffness and the chirality angle are $\eta = 1/4$ and $\beta = -\arctan(1/2)$, respectively. Displacements are magnified by a factor of two.
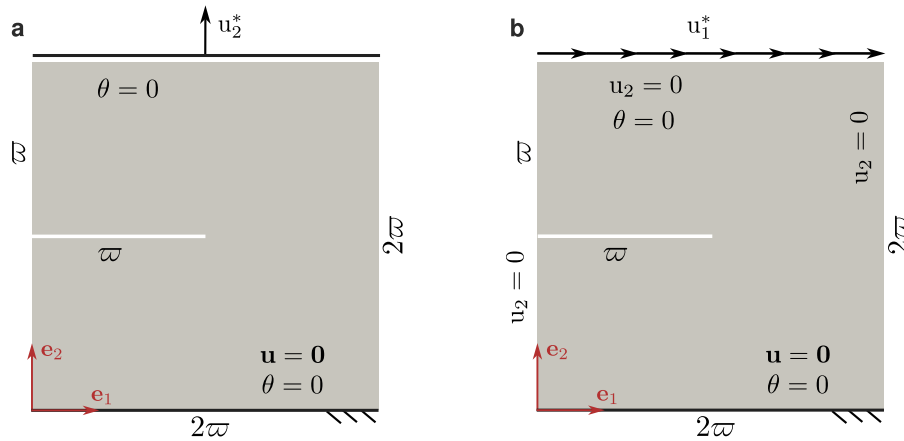

Fig. 21. Quasi-static benchmark fracture tests in micropolar isotropic solids (O(2) invariance): Geometry and boundary conditions of the considered single-edge notched (**a**) tension test and (**b**) shear test.

then obtains

$$w_c = \frac{3\mathscr{G}_c}{2h\delta^3} \tag{105}$$

At this point, it should be noted that in our case fracture is naturally described as a mechanism-based process, since cracks nucleate and grow when a number of bond failures coalesce into a surface and
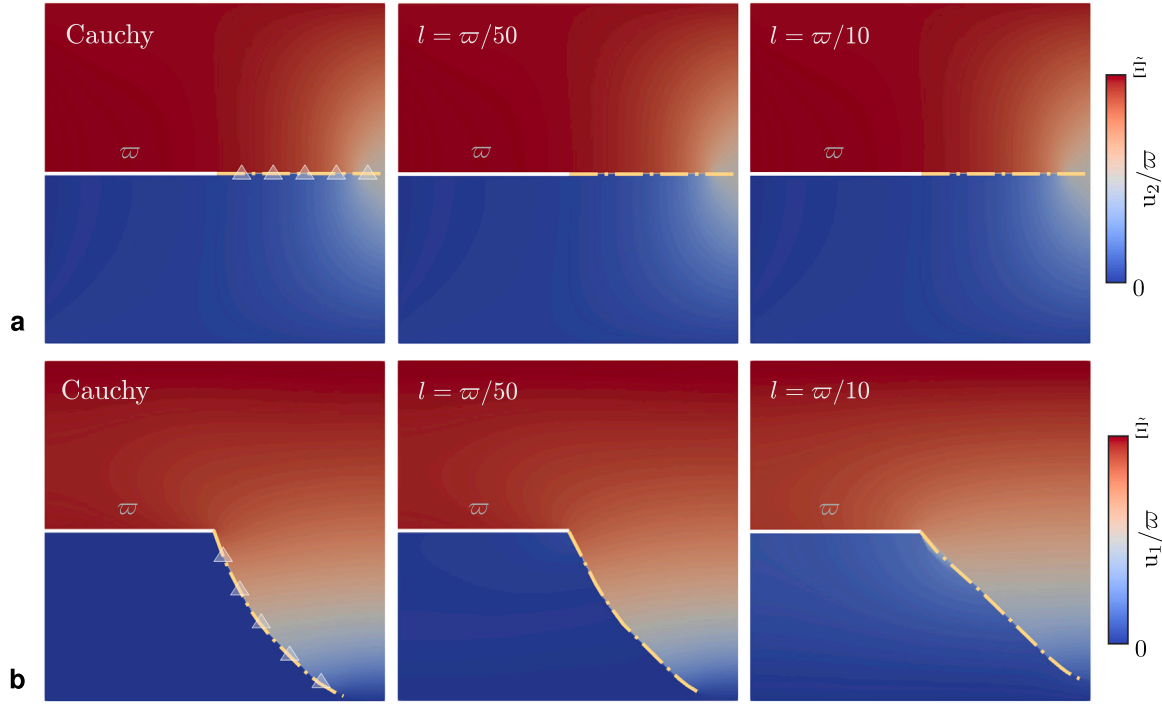
Fig. 22. Quasi-static benchmark fracture tests in micropolar isotropic solids (O(2) invariance): Displacement maps and crack paths obtained by the CM model for the classical single-edge notched tensile (row **a**, with $\Xi = 1.16 \times 10^{-2}$, $\Xi = 1.12 \times 10^{-2}$ and $\Xi = 1.11 \times 10^{-2}$ for the first, second and third column, respectively) and shear (row **b**, with $\Xi = 2.2 \times 10^{-2}$, $\Xi = 2.4 \times 10^{-2}$ and $\Xi = 4 \times 10^{-2}$ for the first, second and third column, respectively) test considering different micropolar internal lengths. CM and phase-field solutions (corresponding to $l_c / 2\varpi = 7.5 \times 10^{-3}$ and denoted by gray shaded triangles) referred to the special case of classical Cauchy solid are also reported for reference.

propagate (Foster et al., 2011). This is very different with respect to phenomenological approaches to fracture as those based on phase-field method. The status of each virtual fiber can be specified by a history-dependent pairwise scalar valued function $\mu(\mathbf{x}, \mathbf{x}', t)$ (Silling and Askari, 2005) such that

$$\mu(\mathbf{x}, \mathbf{x}', t) = \begin{cases} 0, & \mathrm{w}(\mathbf{x}, \mathbf{x}', t) \geq \mathrm{w}_c(\psi, \zeta) \\ 1, & \mathrm{w}(\mathbf{x}, \mathbf{x}', t) < \mathrm{w}_c(\psi, \zeta) \end{cases} \tag{106}$$

where $\mathrm{w}(\mathbf{x}, \mathbf{x}', t) = \mathrm{w}(\psi, t)$. It allows then defining at each position $\mathbf{x}$ and time t a local scalar-valued damage variable associated to the energy-based failure criterion, namely

$$d(\mathbf{x}, t) = 1 - \frac{\int_{H_x} \mu(\mathbf{x}, \mathbf{x}', t) \mathrm{d}\mathbf{x}}{\int_{H_x} \mathrm{d}\mathbf{x}} \tag{107}$$

The square material domain in Fig. 21 is discretized using a uniform grid spacing $\Delta \mathrm{x} = \varpi / 100$, with usual value of the density parameter $m = 5$ (see Section 2.1.1 and Diana (2023)). The pre-existing edge crack of length $\varpi = 0.5$ mm is introduced by removing bonds/virtual fibers that would pass through the corresponding pre-crack pseudo line (Bobaru et al., 2015; Silling and Askari, 2005; Diana and Ballarini, 2020). The (uniform) fracture energy of the material is assumed as $\mathscr{G}_c = 2.7$ N/mm. Numerical analyses are conducted in quasi-static regime using an implicit non-linear solver in displacement control and adaptive-step refinement (Ni et al., 2019; Diana, 2023). Regarding the tensile test, an incremental applied vertical displacement $\Delta u_2 = \Delta u^* = 10^{-5}$ mm is imposed at each pseudo-time step of the simulation, whereas for the single-edge shear test an incremental applied horizontal displacement $\Delta u_2 = \Delta u^*$ is considered. In both the cases, the bottom part of the domain is fixed. For the purposes of this discussion, the special case of classical Cauchy solid ($\kappa = 0$ and vanishing bending internal length l) is also considered for comparison. Regarding Cauchy solution, results obtained using phase-field approach to brittle fracture (based on finite-elements formulation) are also provided for reference. In particular, the phase-field simulations are performed using a FEniCS

Python script with a staggered implementation of the phase field fracture method (Natarajan et al., 2019), particularized to the problems and material object of this study, while assuming two different phase-field regularization lengths l_c with same pseudo-load increments as in CM simulations. Specifically, $l_c / 2\varpi = 1.5 \times 10^{-2}$ and $l_c / 2\varpi = 7.5 \times 10^{-3}$ are considered, which represent well known values in phase-field literature (Miehe et al., 2010; Ambati et al., 2015), the corresponding finite element mesh being characterized by element size of $l_h \approx l_c / 5$ around the potential crack propagation trajectory (Gerasimov and De Lorenzis, 2016).

Considering the pure tensile test, it is noted that the pre-existing crack propagates horizontally till the complete failure of the specimen, with same final crack pattern as for the case of classical Cauchy solid and regardless of l (Fig. 22). Moreover, the corresponding load–deflection curves exhibit very similar response with slight reduction of the critical vertical displacement u_2^* and a slight increase of the global stiffness with increasing micropolar internal length value l (see Fig. 23). This result is expected, as introducing the micro-polar effect does not break the overall symmetry of the boundary value problems in pure Mode I effective global loading (Suh et al., 2020). Conversely, the higher-order constitutive response plays an important role in the single-edge notched shear test as it has significant influence on crack kinking angle and crack propagation direction under Mode II loading. Specifically, the micropolar effect leads to an effective reduction of the obtained kinking angle, with crack propagation direction that bends counterclockwise while reducing its global curvature with increasing the micropolar internal length. Obviously, micropolar effects have profound impact on the corresponding load–deflection curves as the resulting peak load and critical horizontal displacement u_1^* strongly depend on the specific value of the micropolar internal length (Fig. 23). It is worth noting that for the CM model, the crack driving force at the micro-scale $\mathrm{w}(\mathbf{x}, \mathbf{x}', t)$ depends, through the bending micromodulus k_b, on the pairwise curvature measure $\chi(\mathbf{x}, \mathbf{x}', t)$ defined in Eq. (3), which in turn is function of the resulting micro-rotation field $\theta(\mathbf{x}, t)$ *gradient*. Given the asymmetric loading, the macro energy dissipation during the
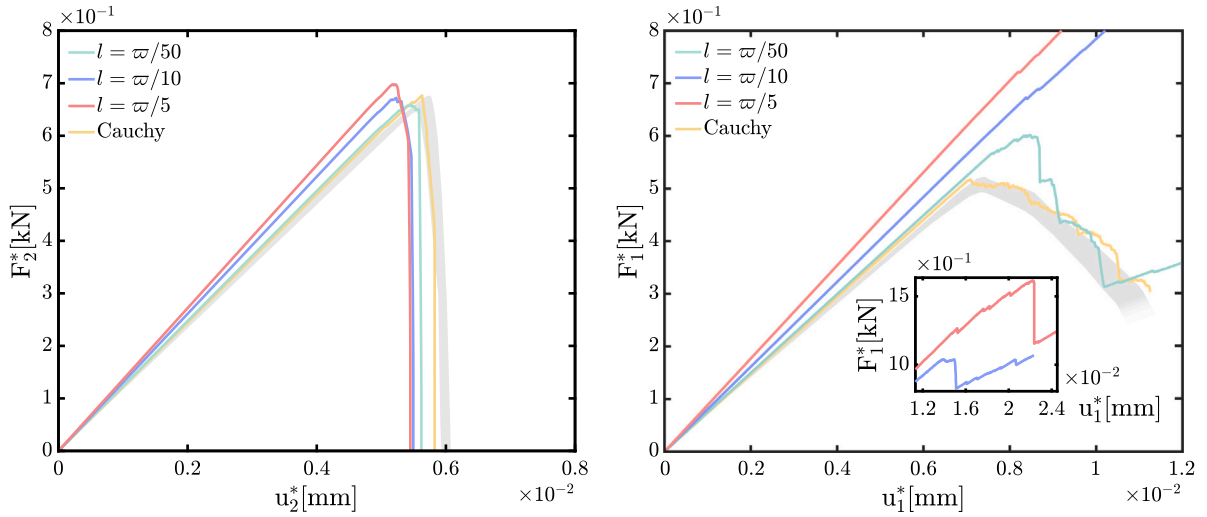
Fig. 23. Quasi-static benchmark fracture tests in micropolar isotropic solids (O(2) invariance): Force–displacement relationships obtained for the classical single-edge notched tension (left) and shear (right) test considering different micropolar internal lengths. CM and phase-field solution (envelope of the results denoted by gray shaded area) referred to the special case of classical (Cauchy) solid are also reported for reference.
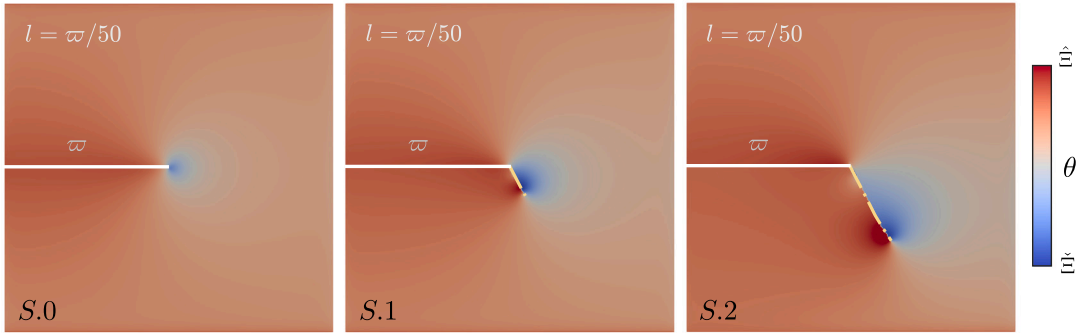

Fig. 24. Quasi-static benchmark fracture tests in micropolar isotropic solids (O(2) invariance): θ field map (with limits $\check{\Xi} = -2.2\times10^{-2}$ and $\hat{\Xi} = 6.0\times10^{-3}$) obtained for the classical single-edge notched shear test considering micropolar internal length $l = \varpi/50$ and corresponding to three different subsequent steps ($S.0$, $u_1^*/\varpi = 1.48\times10^{-2}$; $S.1$, $u_1^*/\varpi = 1.74\times10^{-2}$; $S.2$, $u_1^*/\varpi = 1.82\times10^{-2}$). It can be seen that in the vicinity of the crack front separated particles tend to rotate in opposing directions, them being no longer interlocked after fracture formation.

crack nucleation and propagation in two-dimensional micropolar media under Mode II result to be strongly affected by the specific value of the micropolar bending characteristic length. This affects the resulting crack pattern, which in turn leads to different global response for the same boundary value problem (Suh et al., 2020).

As pointed out by Yavari et al. (2002) and later taken up in Suh et al. (2020), the mechanism of crack propagation in a micropolar continuum consists, in general, of the following steps: (a) crack-tip particles withstand rotation and separation, (b) micro-rotational bonding between adjacent particles at the crack tip breaks and the particles start to rotate with respect to each other, and (c) the particles then move apart and the adjacent set of particles become the next crack-tip particles. Based on this mechanism, if the material is isotropic and homogeneous, the crack path that minimizes the effort required to break the micro-rotational pairwise interaction turns out to be the shortest path towards the boundary (Suh et al., 2020). Furthermore, as shown in Fig. 24, since separated particles are no longer interlocked after fracture formation, they tend to rotate in opposing directions (Suh et al., 2020). Interestingly, the results by CM model for both the cases of tensile and shear single-edge tests result to be consistent with this interpretation as well as with those reported in Suh et al. (2020), Wan et al. (2022), and obtained using different approaches, methods and material properties. Finally, it should be underlined that the CM solutions in terms of load–deflection curves and crack-paths obtained for the reduced case of Cauchy material are in very good agreement with those by phase-field

model here reported, which, differently from the CM model, is based on purely phenomenological considerations (Marigo, 2023) (the envelopes of the two load–deflection curves as referred to the two values of the regularization length considered are reported in Fig. 23, and denoted by gray shaded areas). This is an important and encouraging result as it confirms (see also Diana (2023)) the effectiveness and the natural capabilities of the CM formulation in modeling fracture problems within a mechanism-based framework.

4. Conclusions

In this paper we have presented an analytical continuum-molecular formulation for two-dimensional centrosymmetric micropolar media within the mathematical formalism of a revised peridynamic theory with oriented material points. The model is able to reproduce overall anisotropy as well as chiral effects in architectured materials homogenized as micropolar bi-dimensional solids. In particular, a mechanism-based description of elastic anisotropy is achieved by defining proper direction-dependent micromoduli functions analytically identified based on the formal analogy with the micropolar elastic constitutive tensor. Distinctive chiral effects in micropolar elasticity are reproduced by introducing a directional independent pseudo-scalar pair potential, which turns out to be analytically vanishing when the rotationally invariant part of the corresponding continuum elastic tensor is invariant to mirror reflections as well. This aspect theoretically enables

all the symmetry classes of 2D centrosymmetric micropolar elasticity to be covered. Moreover, the proposed formulation demonstrates sensitivity to elastic bending size-effect as specific property of structured solids homogenized as micropolar continua, and related to the characteristic length of their underlying microstructure. An important consideration is that the model turns out to be characterized by two different length-scale parameters. Specifically, the *constitutive* bending internal length, proper of micropolar elasticity, is conceptually separated with respect to the *intrinsic* non-local character of the model that is related instead to the integral nature of its governing equations. By reducing the horizon size to zero, the *constitutive* length-scale does not vanish, and convergence to the elastic solution of Cosserat continuum is obtained. Essential analogies between continuum-molecular mathematical models and real periodic lattice-like materials associated with a Lagrangian description have been also shown, which may provide new insight for the design of modern micro-architectured solids endowing exotic mechanical properties. The theoretical findings and the effectiveness of the model have been successfully verified through illustrative examples featuring representative cases of structured materials homogenized as micropolar continua.

CRediT authorship contribution statement

Vito Diana: Writing – review & editing, Writing – original draft, Visualization, Validation, Supervision, Software, Methodology, Investigation, Formal analysis, Conceptualization, Data curation, Project administration. **Andrea Bacigalupo:** Writing – review & editing, Supervision, Methodology, Investigation, Conceptualization. **Luigi Gambarotta:** Writing – review & editing, Supervision, Methodology, Investigation, Conceptualization.

Declaration of competing interest

The authors declare that they have no known competing financial interests or personal relationships that could have appeared to influence the work reported in this paper.

Data availability

Data will be made available on request.

Acknowledgments

Appendix. Discretized systems and equations

Considering a meshfree discretization approach (Silling and Askari, 2005; Diana, 2023), the material domain Ω be divided into a set of N sub-domains Δv_p, each of which is associated to a particle p of coordinates x_1^p, x_2^p. A properly defined proximity search algorithm identifies particles q belonging to the p-centered horizon region H_p according to the one-point quadrature scheme proposed by Hu et al. (2010), Seleson (2014) which accounts for partial neighbor intersections (alternatively, other quadrature rules, especially developed for

non-local models, could be adopted (Seleson, 2014; Trask et al., 2019)). The displacements $\mathbf{u}_p = u_1^p \mathbf{e}_1 + u_2^p \mathbf{e}_2, \mathbf{u}_q = u_1^q \mathbf{e}_1 + u_2^q \mathbf{e}_2$ and rotations θ^p, θ^q of the material generic particles p and q can be collected column-wise in vector form as

$$\mathbf{v}_p = \left\{ \begin{array}{ccc} u_1^p & u_2^p & \theta^p \end{array} \right\}^\top, \quad \mathbf{v}_q = \left\{ \begin{array}{ccc} u_1^q & u_2^q & \theta^q \end{array} \right\}^\top \tag{A.1}$$

such that, for each pair of interacting particles p and $q \in H_p$, we can collect column-wise $\mathbf{v}_p$ and $\mathbf{v}_q$ as

$$\mathbf{v}_{pq} = \left\{ \begin{array}{c} \mathbf{v}_p \\ \mathbf{v}_q \end{array} \right\} = \mathbf{R}_{pq}^\top \left\{ \begin{array}{c} \hat{\mathbf{v}}_p \\ \hat{\mathbf{v}}_q \end{array} \right\} = \mathbf{R}_{pq}^\top \hat{\mathbf{v}}_{pq}, \tag{A.2}$$

where $\mathbf{R}_{pq}$ is a properly defined transformation matrix (Diana, 2023), and the displacements and rotations collected column-wise in vector form as

$$\hat{\mathbf{v}}_p = \left\{ \begin{array}{ccc} \hat{u}_1^p & \hat{u}_2^p & \theta^p \end{array} \right\}^\top, \quad \hat{\mathbf{v}}_q = \left\{ \begin{array}{ccc} \hat{u}_1^q & \hat{u}_2^q & \theta^q \end{array} \right\}^\top \tag{A.3}$$

are aligned with the local reference basis $\{\hat{\mathbf{e}}_1, \hat{\mathbf{e}}_2\}$, where the unit vectors $\hat{\mathbf{e}}_1 \equiv \mathbf{n}$ and $\hat{\mathbf{e}}_2 \equiv \mathbf{t}$. The compatibility equation relating the pairwise deformation variables collected in the vector $\mathbf{h}_{pq} = \left\{ \begin{array}{ccc} s_{pq} & \gamma_{pq} & \chi_{pq} \end{array} \right\}^\top$, to the generalized displacements of the interacting particles can be written in compact matrix form as

$$\mathbf{h}_{pq} = \mathbf{B}_{pq} \mathbf{R}_{pq} \mathbf{v}_{pq} = \mathbf{B}_{pq} \hat{\mathbf{v}}_{pq} \tag{A.4}$$

where

$$\mathbf{B}_{pq} = \frac{1}{2\|\xi\|_{pq}} \begin{bmatrix} -2 & 0 & 0 & 2 & 0 & 0 \\ 0 & -2 & -\|\xi\|_{pq} & 0 & 2 & -\|\xi\|_{pq} \\ 0 & 0 & -2 & 0 & 0 & 2 \end{bmatrix} \tag{A.5}$$

being $\|\xi\|_{pq}$ the distance between the generic particles p and q. The pairwise constitutive equation of the virtual fiber is instead

$$\mathbf{r}_{pq} = \mathbf{A}_{pq} \mathbf{h}_{pq} = \mathbf{A}_{pq} \mathbf{B}_{pq} \hat{\mathbf{v}}_{pq}, \tag{A.6}$$

where

$$\mathbf{A}_{pq} = \Lambda_{pq} \begin{bmatrix} k_{\mathrm{n}}^{pq} & k_{\mathrm{a}}^{pq} & 0 \\ k_{\mathrm{a}}^{pq} & k_{\mathrm{t}}^{pq} & 0 \\ 0 & 0 & k_{\mathrm{b}}^{pq} \end{bmatrix} \tag{A.7}$$

defines the specific elastic property of each interaction. It relates the scalar-valued mutual actions defined in Eqs. (5)–(7) and collected in the vector $\mathbf{r}_{pq}$, to the pairwise deformations measures defined by Eqs. (1)–(3). The non-dimensional factor $\Lambda_{pq} = \Lambda_{pq}(\|\xi\|_{pq})$ controls the radial dependence of the non-local interaction between two particles, as specified in Section 2.

As for the balance of linear and angular momentum of the (molecular) continuum (Section 2), the discrete algebraic system of governing equations in elastodynamics, and the analytical expression of the stiffness operator, can be derived from Hamilton's variational principle referred to a closed discretized domain. The variation of the first term of Eq. (9), i.e. $\delta[\int_{t_1}^{t_2} \int_{\Omega} \mathcal{E}(\mathbf{x}, t) \, \mathrm{d}\mathbf{x} \, \mathrm{d}t]$ can be written in discrete form as

$$\delta \left[\int_{t_1}^{t_2} \sum_{p=1}^{N} \frac{1}{2} \dot{\mathbf{v}}_p^\top \mathbf{P}_p \dot{\mathbf{v}}_p \Delta v_p \, \mathrm{d}t \right] = - \int_{t_1}^{t_2} \sum_{p=1}^{N} \delta \mathbf{v}_p^\top \mathbf{P}_p \ddot{\mathbf{v}}_p \Delta v_p \, \mathrm{d}t \tag{A.8}$$

where integration-by-parts is used between the first and the second steps, and

$$\mathbf{P}_p = \mathrm{diag}\{\rho_p \quad \rho_p \quad \varrho_p\} \tag{A.9}$$

The variation of the second term of Eq. (9), i.e. $\delta[\int_{t_1}^{t_2} \int_{\Omega} \mathcal{V}(\mathbf{x}, t) \, \mathrm{d}\mathbf{x} \, \mathrm{d}t]$, can be treated in discrete form as

$$\int_{t_1}^{t_2} \sum_{p=1}^{N} \delta \mathbf{v}_p^\top \mathbf{b}_p \, \Delta v_p \, \mathrm{d}t \tag{A.10}$$

where $\mathbf{b}_p = \{b_1^p \quad b_2^p \quad c^p\}^T$ is the vector of body forces and body couples applied at particle p in the global reference system of unit vectors $\mathbf{e}_1, \mathbf{e}_2$. Finally, considering Eq. (4), the last term of Eq. (9),

i.e. $\delta[\int_{t_1}^{t_2} \int_{\Omega} \mathcal{W}(\mathbf{x}, t)\, d\mathbf{x}\, dt]$, can be written instead for a discretized body as

$$\delta\left[\frac{1}{2}\int_{t_1}^{t_2}\sum_{p=1}^{N}\sum_{q=1}^{H}\frac{\|\boldsymbol{\xi}\|_{pq}}{2}\alpha_{pq}\Delta v_q \Delta v_p \mathbf{v}_{pq}^{\top}\left[\mathbf{R}_{pq}^{\top}\mathbf{B}_{pq}^{\top}\mathbf{A}_{pq}\mathbf{B}_{pq}\mathbf{R}_{pq}\right]\mathbf{v}_{pq}\,dt\right] \quad \text{(A.11)}$$

where H denotes the number of particles q within the p-centered horizon δ, while α_{pq} is the partial sub-domain factor for Δv_q related to the specific quadrature rule adopted (Seleson, 2014). Considering Eq. (9) together with Eqs. (A.8), (A.10) and (A.11), the stationary condition $\delta\mathcal{H} = 0$ gives

$$\bigwedge_{(p,q)=(1,1)}^{(N,H)}\left[\mathbf{L}_{pq}\mathbf{P}_p\ddot{\mathbf{v}}_p\Delta v_p - \mathbf{L}_{pq}\mathbf{b}_p\Delta v_p \right.$$
$$\left. + \frac{\|\boldsymbol{\xi}\|_{pq}}{2}\left[\mathbf{R}_{pq}^{\top}\mathbf{B}_{pq}^{\top}\mathbf{A}_{pq}\mathbf{B}_{pq}\mathbf{R}_{pq}\alpha_{pq}\Delta v_q \ \Delta v_p\right]\mathbf{L}_{pq}\mathbf{v}_p\right] = \mathbf{0} \quad \text{(A.12)}$$

where $\mathbf{L}_{pq} = \begin{bmatrix}\mathbf{I}_3 & \mathbf{0}_3\end{bmatrix}^{\top}$ is a specific topology incidence matrix for non-pairwise defined matrices and vectors (Diana et al., 2022). The assembly operator $\bigwedge$ replaces the double sum symbol, and is here introduced so that each algebraic object is added to the appropriate location in properly defined global matrices and vectors (Hughes, 2012). In this way, Eq. (A.12) can be then rewritten in compact form as

$$\mathbf{M}\ddot{\mathbf{v}} + \mathbf{K}\mathbf{v} = \mathbf{p} \quad \text{(A.13)}$$

where the global mass matrix is given by

$$\mathbf{M} = \bigwedge_{(p,q)=(1,1)}^{(N,H)}\mathbf{L}_{pq}\mathbf{P}_p\Delta v_p \quad \text{(A.14)}$$

whereas the stiffness operator in global coordinate system corresponding to the whole body is defined as

$$\mathbf{K} = \bigwedge_{(p,q)=(1,1)}^{(N,H)}\frac{\|\boldsymbol{\xi}\|_{pq}}{2}\left[\mathbf{R}_{pq}^{\top}\mathbf{B}_{pq}^{\top}\mathbf{A}_{pq}\mathbf{B}_{pq}\mathbf{R}_{pq}\alpha_{pq}\Delta v_q \ \Delta v_p\right] \quad \text{(A.15)}$$

The vector of global generalized body forces and global generalized displacements are

$$\mathbf{p} = \bigwedge_{(p,q)=(1,1)}^{(N,H)}\mathbf{L}_{pq}\mathbf{b}_p\Delta v_p, \qquad \mathbf{v} = \bigwedge_{(p,q)=(1,1)}^{(N,H)}\mathbf{L}_{pq}\mathbf{v}_p, \quad \text{(A.16)}$$

respectively. Quasi-static conditions adopted in this work are obtained neglecting the inertial terms in Eq. (A.13).

References

Ambati, M., Gerasimov, T., De Lorenzis, L., 2015. A review on phase-field models of Brittle fracture and a new fast hybrid formulation. Comput. Mech. 55, 383–405.

Auffray, N., El Ouafa, S., Rosi, G., Desmorat, B., 2022. Anisotropic structure of two-dimensional linear Cosserat elasticity. Math. Mech. Complex Syst..

Auffray, N., Ropars, P., 2016. Invariant-based reconstruction of bidimensional elasticity tensors. Int. J. Solids Struct. 87, 183–193.

Bacigalupo, A., Diana, V., Gambarotta, L., 2023. Energy absorbing multilayered self-recovering metamaterials with chiral topology. Int. J. Solids Struct. 273, 112213.

Bacigalupo, A., Gambarotta, L., 2010. Second-order computational homogenization of heterogeneous materials with periodic microstructure. ZAMM-J. Appl. Math. Mech./Zeitschrift für Angew. Math. Mech. 90 (10–11), 796–811.

Bacigalupo, A., Gambarotta, L., 2014. Homogenization of periodic hexa-and tetrachiral cellular solids. Compos. Struct. 116, 461–476.

Bacigalupo, A., Gambarotta, L., 2017. Dispersive wave propagation in two-dimensional rigid periodic blocky materials with elastic interfaces. J. Mech. Phys. Solids 102, 165–186.

Bacigalupo, A., Gambarotta, L., 2020. Chiral two-dimensional periodic blocky materials with elastic interfaces: Auxetic and acoustic properties. Extreme Mech. Lett. 39, 100769.

Bacigalupo, A., Gambarotta, L., Lepidi, M., 2021. Thermodynamically consistent non-local continualization for Masonry-like systems. Int. J. Mech. Sci. 205, 106538.

Ballarini, R., Diana, V., Biolzi, L., Casolo, S., 2018. Bond-based peridynamic modelling of singular and nonsingular crack-tip fields. Meccanica 53 (14), 3495–3515.

Bertoldi, K., Bigoni, D., Drugan, W., 2008. Nacre: An orthotropic and bimodular elastic material. Compos. Sci. Technol. 68 (6), 1363–1375.

Bobaru, F., 2011. Peridynamics and multiscale modeling. Int. J. Multiscale Comput. Eng. 9 (6), vii–ix.

Bobaru, F., Foster, J., Geubelle, P., Silling, S., 2015. Handbook of peridynamic modeling. In: Advances in Applied Mathematics. CRC Press.

Bobaru, F., Yang, M., Alves, L.F., Silling, S.A., Askari, E., Xu, J., 2009. Convergence, adaptive refinement, and scaling in 1D peridynamics. Internat. J. Numer. Methods Engrg. 77 (6), 852–877.

Boys, B., Dodwell, T., Hobbs, M., Girolami, M., 2021. PeriPy - A high performance OpenCL peridynamics package. Comput. Methods Appl. Mech. Engrg. 386, 114085.

Capecchi, D., Ruta, G., 2015. The theory of elasticity in the 19th century. In: Strength of Materials and Theory of Elasticity in 19th Century Italy: A Brief Account of the History of Mechanics of Solids and Structures. Springer International Publishing, Springer International Publishing, pp. 1–81.

Capecchi, D., Ruta, G., Trovalusci, P., 2010. From classical to Voigt's molecular models in elasticity. Arch. Hist. Exact Sci. 64 (5), 525–559.

Casolo, S., 2021. A linear-elastic heuristic-molecular modelling for plane isotropic micropolar and auxetic materials. Int. J. Solids Struct. 224, 111042.

Chen, Y., Liu, X., Hu, G., 2014a. Micropolar modeling of planar orthotropic rectangular chiral lattices. Comptes Rendus Mécanique 342 (5), 273–283.

Chen, Y., Liu, X.N., Hu, G.K., Sun, Q.P., Zheng, Q.S., 2014b. Micropolar continuum modelling of bi-dimensional tetrachiral lattices. Proc. R. Soc. A: Math. Phys. Eng. Sci. 470 (2165), 20130734.

Chen, Z., Wan, J., Chu, X., Liu, H., 2019. Two cosserat peridynamic models and numerical simulation of crack propagation. Eng. Fract. Mech. 211, 341–361.

Chowdhury, S.R., Rahaman, M.M., Roy, D., Sundaram, N., 2015. A micropolar peridynamic theory in linear elasticity. Int. J. Solids Struct. 59, 171–182.

Cosserat, E.M.P., Cosserat, F., 1909. Théorie des corps déformables. A. Hermann et fils.

Cui, Z., Ju, J., 2022. Mechanical coupling effects of 2D lattices uncovered by decoupled micropolar elasticity tensor and symmetry operation. J. Mech. Phys. Solids 167, 105012.

Deng, G., Dargush, G.F., 2021. Mixed variational principle and finite element formulation for couple stress elastostatics. Int. J. Mech. Sci. 202, 106497.

Desmorat, B., Olive, M., Auffray, N., Desmorat, R., Kolev, B., 2023. Computation of minimal covariants bases for 2D coupled constitutive laws. Internat. J. Engrg. Sci. 191, 103880.

Di Paola, M., Failla, G., Pirrotta, A., Sofi, A., Zingales, M., 2013. The mechanically based non-local elasticity: An overview of main results and future challenges. Phil. Trans. R. Soc. A 371 (1993), 20120433.

Diana, V., 2023. Anisotropic continuum-molecular models: A unified framework based on pair potentials for elasticity, fracture and diffusion-type problems. Arch. Comput. Methods Eng. 30, 1305–1344.

Diana, V., Bacigalupo, A., Gambarotta, L., 2023. Thermodinamically-consistent dynamic continualization of block-lattice materials. Int. J. Solids Struct. 262–263, 112050.

Diana, V., Bacigalupo, A., Gambarotta, L., 2024. Dynamic continualization of Masonry-like structured materials. Math. Mech. Solids 29 (3), 577–595.

Diana, V., Bacigalupo, A., Lepidi, M., Gambarotta, L., 2022. Anisotropic peridynamics for homogenized microstructured materials. Comput. Methods Appl. Mech. Engrg. 392 (114704).

Diana, V., Ballarini, R., 2020. Crack kinking in isotropic and orthotropic micropolar peridynamic solids. Int. J. Solids Struct. 196–197, 76–98.

Diana, V., Carvelli, V., 2021. A continuum-molecular model for anisotropic electrically conductive materials. Int. J. Mech. Sci. 211, 106759.

Diana, V., Casolo, S., 2019. A bond-based micropolar peridynamic model with shear deformability: Elasticity, failure properties and initial yield domains. Int. J. Solids Struct. 160, 201–231.

DiCarlo, A., Podio-Guidugli, P., 2021. From point particles to body points. Math. Eng. 4 (1), 1–29.

Ericksen, J., 1984. The Cauchy and born hypotheses for crystals. In: Gurtin, M.E. (Ed.), Phase Transformations and Material Instabilities in Solids. Academic Press, pp. 61–77.

Ericksen, J., 2008. On the Cauchy—Born rule. Math. Mech. Solids 13 (3–4), 199–220.

Eringen, A.C., 1966a. Linear theory of micropolar elasticity. J. Math. Mech. 909–923.

Eringen, A., 1966b. A unified theory of thermomechanical materials. Internat. J. Engrg. Sci. 4 (2), 179–202.

Eringen, A., 1972. Nonlocal polar elastic continua. Internat. J. Engrg. Sci. 10 (1), 1–16.

Eringen, A., Edelen, D., 1972. On nonlocal elasticity. Internat. J. Engrg. Sci. 10 (3), 233–248.

Evans, K.E., Alderson, A., 2000. Auxetic materials: Functional materials and structures from lateral thinking!. Adv. Mater. 12 (9), 617–628.

Fleck, N.A., Deshpande, V.S., Ashby, M.F., 2010. Micro-architectured materials: Past, present and future. Proc. R. Soc. A: Math. Phys. Eng. Sci. 466 (2121), 2495–2516.

Fleck, N.A., Qiu, X., 2007. The damage tolerance of elastic–brittle, two-dimensional isotropic lattices. J. Mech. Phys. Solids 55 (3), 562–588.

Forest, S., 2005. Mechanics of Cosserat Media—An Introduction. Ecole des Mines de Paris, Paris, pp. 1–20.

Forte, S., Vianello, M., 1996. Symmetry classes for elasticity tensors. J. Elasticity 43, 81–108.

Foster, J., Silling, S., Chen, W., 2011. An energy based failure criterion for use with peridynamic states. Int. J. Multiscale Comput. Eng. 9 (6), 675–687.

Gao, H., Klein, P., 1998. Numerical simulation of crack growth in an isotropic solid with randomized internal cohesive bonds. J. Mech. Phys. Solids 46 (2), 187–218.

Gerasimov, T., De Lorenzis, L., 2016. A line search assisted monolithic approach for phase-field computing of Brittle fracture. Comput. Methods Appl. Mech. Engrg. 312, 276–303, Phase Field Approaches to Fracture.

Gerstle, W., Sau, N., Silling, S., 2007. Peridynamic modeling of concrete structures. Nucl. Eng. Des. 237 (12–13), 1250–1258.

Giorgio, I., dell'Isola, F., Misra, A., 2020. Chirality in 2D cosserat media related to stretch-micro-rotation coupling with links to granular micromechanics. Int. J. Solids Struct. 202, 28–38.

Giorgio, I., Hild, F., Gerami, E., dell'Isola, F., Misra, A., 2022. Experimental verification of 2D Cosserat chirality with stretch-micro-rotation coupling in orthotropic metamaterials with granular motif. Mech. Res. Commun. 126, 104020.

Greco, F., Leonetti, L., Pranno, A., Rudykh, S., 2020. Mechanical behavior of bio-inspired nacre-like composites: A hybrid multiscale modeling approach. Compos. Struct. 233, 111625.

Green, A.E., Rivlin, R.S., 1964. Multipolar continuum mechanics. Arch. Rational Mech. Anal. 17, 113–147.

Hu, W., Ha, Y., Bobaru, F., 2010. Numerical Integration in Peridynamics. Tech. Rep., University of Nebraska-Lincoln, Department of Mechanical & Materials Engineering.

Huang, K.-X., Shui, G.-S., Wang, Y.-Z., Wang, Y.-S., 2023. Kinking prohibition enhancement of interface crack in artificial periodic structures with local resonators. J. Mech. Phys. Solids 180, 105421.

Hughes, T.J., 2012. The Finite Element Method: Linear Static and Dynamic Finite Element Analysis. Courier Corporation.

Javili, A., McBride, A., Steinmann, P., 2019. Continuum-kinematics-inspired peridynamics. Mechanical problems. J. Mech. Phys. Solids 131, 125–146.

Kröner, E., 1967. Elasticity theory of materials with long range cohesive forces. Int. J. Solids Struct. 3 (5), 731–742.

Kumar, R.S., McDowell, D.L., 2004. Generalized continuum modeling of 2-D periodic cellular solids. Int. J. Solids Struct. 41 (26), 7399–7422.

Kunin, I.A., 1982. Elastic Media with Microstructure, vol. 26, Springer Berlin Heidelberg, New York.

Lakes, R., 2001. Elastic and viscoelastic behavior of chiral materials. Int. J. Mech. Sci. 43 (7), 1579–1589.

Le, Q.V., Bobaru, F., 2017. Surface corrections for peridynamic models in elasticity and fracture. Comput. Mech..

Liu, X., Huang, G., Hu, G., 2012. Chiral effect in plane isotropic micropolar elasticity and its application to chiral lattices. J. Mech. Phys. Solids 60 (11), 1907–1921.

Liu, Y., St-Pierre, L., Fleck, N., Deshpande, V., Srivastava, A., 2020. High fracture toughness micro-architectured materials. J. Mech. Phys. Solids 143, 104060.

Love, A., 1944. A Treatise on the Mathematical Theory of Elasticity. Dover, New York.

Marigo, J.-J., 2023. Modelling of fracture by cohesive force models: A path to pursue. Eur. J. Mech. A Solids 102, 105088.

Miehe, C., Hofacker, M., Welschinger, F., 2010. A phase field model for rate-independent crack propagation: Robust algorithmic implementation based on operator splits. Comput. Methods Appl. Mech. Engrg. 199 (45), 2765–2778.

Mindlin, R., Eshel, N., 1968. On first strain-gradient theories in linear elasticity. Int. J. Solids Struct. 4 (1), 109–124.

Mindlin, R.D., et al., 1963. Microstructure in Linear Elasticity. Columbia University New York.

Nakamura, S., Lakes, R., 1995. Finite element analysis of Saint-Venant end effects in micropolar elastic solids. Eng. Comput..

Natarajan, S., Annabattula, R.K., Martínez-Pañeda, E., et al., 2019. Phase field modelling of crack propagation in functionally graded materials. Composites B 169, 239–248.

Ni, T., Zaccariotto, M., Zhu, Q.-Z., Galvanetto, U., 2019. Static solution of crack propagation problems in peridynamics. Comput. Methods Appl. Mech. Engrg. 346, 126–151.

Obrezkov, L., Matikainen, M.K., Kouhia, R., 2022. Micropolar beam-like structures under large deformation. Int. J. Solids Struct. 254, 111899.

Omidi, M., St-Pierre, L., 2023. Fracture toughness of semi-regular lattices. Int. J. Solids Struct. 270, 112233.

Prall, D., Lakes, R., 1997. Properties of a chiral honeycomb with a Poisson's ratio of -1. Int. J. Mech. Sci. 39 (3), 305–314.

Quintana-Alonso, I., Fleck, N.A., 2009. Fracture of Brittle lattice materials: A review. In: Major Accomplishments in Composite Materials and Sandwich Structures. Springer, pp. 799–816.

Rezaei, S., Mianroodi, J.R., Brepols, T., Reese, S., 2021. Direction-dependent fracture in solids: Atomistically calibrated phase-field and cohesive zone model. J. Mech. Phys. Solids 147, 104253.

Seleson, P., 2014. Improved one-point quadrature algorithms for two-dimensional peridynamic models based on analytical calculations. Comput. Methods Appl. Mech. Engrg. 282, 184–217.

Seleson, P., Parks, M., 2011. On the role of the influence function in the peridynamic theory. Int. J. Multiscale Comput. Eng. 9 (6), 689–706.

Silling, S., 2000. Reformulation of elasticity theory for discontinuities and long-range forces. J. Mech. Phys. Solids 48 (1), 175–209.

Silling, S., Askari, E., 2005. A meshfree method based on the peridynamic model of solid mechanics. Comput. Struct. 83 (17–18), 1526–1535.

Silling, S., Epton, M., Weckner, O., Xu, J., Askari, E., 2007. Peridynamic states and constitutive modeling. J. Elasticity 88 (2), 151–184.

Silling, S., Lehoucq, R., 2008. Convergence of peridynamics to classical elasticity theory. J. Elasticity 93 (1), 13–37.

Spencer, A., 1970. A note on the decomposition of tensors into traceless symmetric tensors. Internat. J. Engrg. Sci. 8 (6), 475–481.

Stakgold, I., 1950. The Cauchy relations in a molecular theory of elasticity. Quart. Appl. Math. 8 (2), 169–186.

Suh, H.S., Sun, W., O'Connor, D.T., 2020. A phase field model for cohesive fracture in micropolar continua. Comput. Methods Appl. Mech. Engrg. 369, 113181.

Tadmor, E.B., Ortiz, M., Phillips, R., 1996. Quasicontinuum analysis of defects in solids. Phil. Mag. A 73 (6), 1529–1563.

Trask, N., You, H., Yu, Y., Parks, M.L., 2019. An asymptotically compatible meshfree quadrature rule for nonlocal problems with applications to peridynamics. Comput. Methods Appl. Mech. Engrg. 343, 151–165.

Trovalusci, P., Masiani, R., 1999. Material symmetries of micropolar continua equivalent to lattices. Int. J. Solids Struct. 36 (14), 2091–2108.

Truesdell, C.A., 1992. Cauchy and the modern mechanics of continua. Revue d'histoire des sci. 5–24.

Truesdell, C., Toupin, R., 1960. The classical field theories. In: Flügge, S. (Ed.), Principles of Classical Mechanics and Field Theory / Prinzipien Der Klassischen Mechanik Und Feldtheorie. Springer Berlin Heidelberg, Berlin, Heidelberg, pp. 226–858.

Voigt, W., 1887. Theoretische Studien über die Elastizitätsverhältnisse der Krystalle. Abh. Ges. Wiss. Gottingen 34, 3–51.

Voigt, W., 1900. L'état actuel de nos connoissances sur l'élasticité des cristaux. In: Guillaume, C.-E., Poincaré, L. (Eds.), Rapports présentes au Congrés international de Physique. Gautier-Villars, Paris, pp. 277–347.

Voigt, W., 1928. Lehrbuch der Kristallphysik. Teubner, Leipzig.

Wan, J., Yang, D., Chu, X., Qu, W., 2022. A micropolar peridynamic differential operator and simulation of crack propagation. Eng. Fract. Mech. 269.

Warren, T.L., Silling, S.A., Askari, A., Weckner, O., Epton, M.A., Xu, J., 2009. A non-ordinary state-based peridynamic method to model solid material deformation and fracture. Int. J. Solids Struct. 46 (5), 1186–1195.

Wu, Q., Gao, Q., 2023. The symplectic approach for analytical solution of micropolar plane stress problem. Int. J. Solids Struct. 264, 112095.

Yavari, A., Sarkani, S., Moyer, Jr., E., 2002. On fractal cracks in micropolar elastic solids. J. Appl. Mech. 69 (1), 45–54.

Zhang, H., Wang, H., Liu, G., 2005. Quadrilateral isoparametric finite elements for plane elastic Cosserat bodies. Acta Mech. Sin. 21 (4), 388–394.

Zhou, L., Zhu, S., Zhu, Z., 2023. Cosserat ordinary state-based peridynamic model and numerical simulation of rock fracture. Comput. Geotech. 155.

Zou, W.N., Zheng, Q.S., Du, D.X., Rychlewski, J., 2001. Orthogonal irreducible decompositions of tensors of high orders. Math. Mech. Solids 6 (3), 249–267.